Nucleic Acids Research, 2025, **53**, gkaf183
https://doi.org/10.1093/nar/gkaf183
RNA and RNA-protein complexes

Syn-tasiR-VIGS: virus-based targeted RNAi in plants by synthetic trans-acting small interfering RNAs derived from minimal precursors

Adriana E. Cisneros [1,†], Ana Alarcia [1,†], Juan José Llorens-Gámez [1], Ana Puertes [1], María Juárez-Molina [1], Anamarija Primc [1,2], Alberto Carbonell [1,*]

[1]Instituto de Biología Molecular y Celular de Plantas (Consejo Superior de Investigaciones Científicas–Universitat Politècnica de València), 46022 Valencia, Spain
[2]Present address: Center for Organismal Studies (COS), University of Heidelberg, 69120 Heidelberg, Germany

[*]To whom correspondence should be addressed. Email: acarbonell@ibmcp.upv.es
[†]The first two authors should be regarded as Joint First Authors.

Abstract

Synthetic trans-acting small interfering RNAs (syn-tasiRNAs) are 21-nucleotide (nt) small RNAs designed to silence plant transcripts with high specificity. Their use as biotechnological tools for functional genomics and crop improvement is limited by the need to transgenically express long *TAS* precursors to produce syn-tasiRNAs *in vivo*. Here, we show that authentic and highly effective syn-tasiRNAs can be produced from minimal, non-*TAS* precursors consisting of a 22-nt endogenous microRNA target site, an 11-nt spacer, and the 21 nt syn-tasiRNA sequence(s). These minimal precursors, when transgenically expressed in *Arabidopsis thaliana* and *Nicotiana benthamiana*, generated highly phased syn-tasiRNAs that silenced one or multiple plant genes with high efficacy. Remarkably, minimal but not full-length *TAS* precursors produced authentic syn-tasiRNAs and induced widespread gene silencing in *N. benthamiana* when expressed from an RNA virus, which can be applied by spraying infectious crude extracts onto leaves in a transgene-free manner. This strategy, named syn-tasiRNA-based virus-induced gene silencing (syn-tasiR-VIGS), was further used to vaccinate plants against a pathogenic virus, resulting in complete plant immunization. Our results reveal that syn-tasiRNA precursors can be significantly shortened without compromising silencing efficacy, and that syn-tasiR-VIGS represents a versatile, scalable, and nontransgenic platform for precision RNA interference and antiviral vaccination in plants.

Graphical abstract

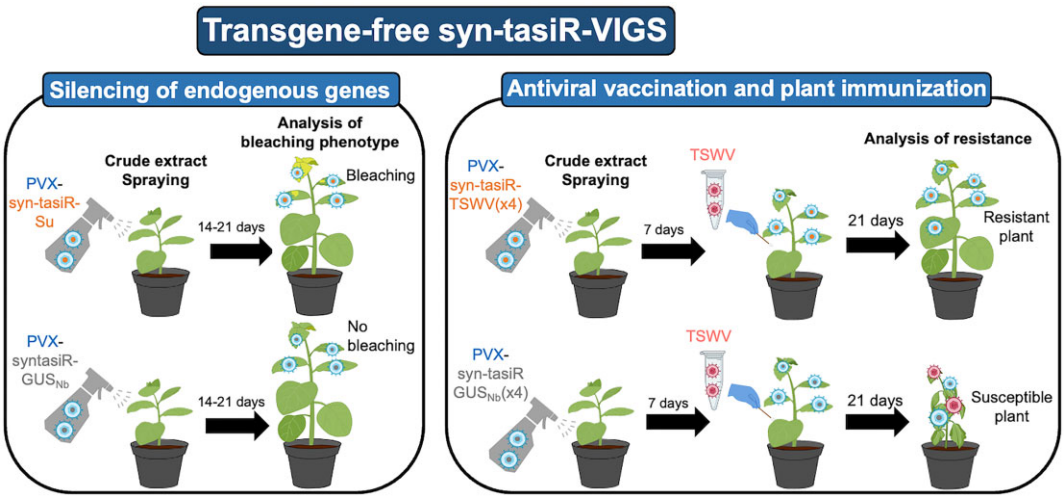

Introduction

Classic RNA interference (RNAi) strategies for gene silencing rely on the processing of double-stranded RNA (dsRNA) by Dicer ribonucleases into small interfering RNAs (siRNAs) [1, 2]. One strand of the duplex, the guide strand, is loaded into an ARGONAUTE (AGO) protein, forming an RNA-induced silencing complex that binds and silences target RNAs with high sequence complementarity to the guide strand [2, 3]. Despite their widespread use, classic RNAi strategies present a major limitation, which is the lack of high specificity due to the generation of an uncontrolled array of siRNAs of unpredicted sequence and size that may acciden-

Received: December 2, 2024. **Revised:** January 22, 2025. **Editorial Decision:** February 18, 2025. **Accepted:** February 24, 2025

tally bind to cellular transcripts and cause toxic off-target effects [4].

In plants, second generation RNAi tools are based on 21-nucleotide (nt) single-stranded RNA molecules, named artificial soluble RNAs (art-sRNAs), computationally designed to bind and cleave target RNAs with high specificity and no off-target effects [5]. There are two main classes of art-sRNAs: artificial microRNAs (amiRNAs) and synthetic trans-acting siRNAs (syn-tasiRNAs), which are functionally similar but differ in their biogenesis pathway. AmiRNAs are typically produced from *MIR* transgenes, where endogenous microRNA (miRNA) and miRNA* sequences are replaced with amiRNA and amiRNA* sequences. While amiRNAs are often designed to target a single transcript, a unique feature of syn-tasiRNAs is their multiplexing capability, allowing the production of multiple syn-tasiRNAs from a single precursor and, therefore, the multitargeting of different sites within one or multiple target RNAs [6]. Syn-tasiRNAs are typically produced from *TAS* transgenes in which the endogenous tasiRNA sequences are replaced by one or more 21-nt syn-tasiRNA sequences in tandem, designed to target the gene(s) of interest [6, 7]. These transgenes are transcribed in the nucleus by DNA-DEPENDENT RNA POLYMERASE II into a primary *TAS* transcript (or *TAS* precursor) that includes a 5′ cap structure, a poly(A) tail and a target site (TS) specific for a miRNA, usually of 22 nt [8, 9]. Once the *TAS* precursor is exported to the cytoplasm, a miRNA/AGO complex mediates the endonucleolytic cleavage of the *TAS* precursor. Next, SUPRESSOR OF GENE SILENCING 3 (SGS3) stabilizes one of the cleaved *TAS* fragments, which is then used by RNA-DEPENDENT RNA POLYMERASE 6 (RDR6) to synthesize a dsRNA molecule. This dsRNA is processed into phased, 21-nt syn-tasiRNA duplexes by DICER LIKE 4 (DCL4), as observed for endogenous tasiRNAs [10, 11]. Finally, HUA ENHANCER1 (HEN1) methylates the 3′ end of both strands of the duplex [12], and the guide strand is loaded into AGO1 to cleave or translationally repress complementary RNAs.

Arabidopsis thaliana (Arabidopsis) has eight *TAS* loci, belonging to four gene families (*AtTAS1a-c*, *AtTAS2*, *AtTAS3a-c*, and *AtTAS4*). Syn-tasiRNAs have been produced in plants from transgenes including modified *AtTAS1a*, *AtTAS1c*, and *AtTAS3a* precursors [13–15]. *AtTAS1c* is the preferred precursor, as it is accurately processed and yields high levels of authentic syn-tasiRNAs [16, 17] that efficiently silence endogenous genes [18] and confer resistance to plant viruses and viroids [19, 20]. Importantly, *AtTAS1c*-derived syn-tasiRNA biogenesis is triggered by the Arabidopsis 22-nt miRNA miR173a, which is only present in this species and its close relatives. Therefore, in non-Arabidopsis species, the *AtMIR173a* gene must be co-expressed with the *AtTAS1c* precursor to produce syn-tasiRNAs.

Syn-tasiRNAs possess unique features that have boosted their application for functional genomics and crop improvement [7, 21]: (i) their multiplexing capability enables the simultaneous production of multiple syn-tasiRNAs from a single precursor for multitargeting; (ii) their expression at different precursor positions allows for fine-tuning targeted RNAi efficacy [18]; and (iii) the development of fast-forward methodologies for their design and cloning accelerates the generation of syn-tasiRNA constructs [16, 22–24]. Still, a major limitation of syn-tasiRNA technology is the need for integrating *TAS*-based transgenes into plant genomes, a process that is time-consuming and raises regulatory concerns about the generation of genetically-modified plants [25]. Also, another limitation is the use of relatively long *TAS*-based precursors, which (i) may increase the cost of the *in vitro* or bacterial synthesis of RNA precursors for topical delivery, and (ii) may not be stable when incorporated into viral vectors, as reported recently for full-length amiRNA precursors [26]. Therefore, further optimization of the syn-tasiRNA technology is required to expand its applicability while avoiding the generation of transgenic plants.

Here, we show that authentic and highly effective syn-tasiRNAs can be produced from minimal, non-*TAS* precursors consisting of a 22-nt endogenous microRNA TS, an 11-nt spacer and the 21 nt syn-tasiRNA sequence(s). These minimal precursors were functional when expressed in transgenic plants or from an RNA virus, allowing for multi-gene silencing and for plant antiviral vaccination in a DNA-free manner.

Materials and methods

Plant species and growth conditions

Nicotiana benthamiana plants were grown in a growth chamber at 25°C with a 12 h-light/12 h dark photoperiod. Arabidopsis Col-0 plants were grown in a growth chamber at 22°C with a 16 h-light/8 h-dark photoperiod. Genetic transformation of Arabidopsis was done following the floral dip method [27] using the *Agrobacterium tumefaciens* GV3101 strain. T1 transgenic Arabidopsis were done as described [18]. A Nikon D3000 digital camera with AF-S DX NIKKOR 18–55 mm f/3.5–5.6G VR lens was used for photographing plants.

Arabidopsis phenotyping

Arabidopsis phenotyping analyses were performed in blind as described [18]. Briefly, the flowering time of each independent line results from the number of days elapsed since seed plating to first bud opening (or 'days to flowering'). The 'Ft' phenotype was defined as a higher 'days to flowering' value when compared to the average 'days to flowering' value of the *35S:TAS-GUS* control set. The 'CH42' phenotype was scored in 10-day-old seedlings and was considered 'weak', 'intermediate', or 'severe' if seedlings had more than two leaves, exactly two leaves or no leaves at all (only two cotyledons), respectively. A line was considered to have a 'TRY' phenotype when presenting a visually obvious higher number of trichomes in rosette leaves of 14-day-old seedlings when compared to transformants of the *35S:TAS-GUS* control set.

Artificial small RNA design

Syn-tasiR-GUS$_{At}$, syn-tasiR-FT, syn-tasiR-CH42, syn-tasiR-TRY, syn-tasiR-GUS$_{Nb}$, syn-tasiR-Su, syn-tasiR-GUS$_{Nb}$-1/amiR-GUS$_{Nb}$, syn-tasiR-GUS$_{Nb}$-2, syn-tasiR-TSWV-1/amiR-TSWV, syn-tasiR-TSWV-2, syn-tasiR-TSWV-3, and syn-tasiR-TSWV-4 guide sequences were described before [17–20, 28].

DNA constructs

Oligonucleotides AC-674 and AC-675 were annealed and ligated into *pENTR-D-TOPO* (Invitrogen) following manufacturer's instructions to generate *pENTR-BB* including two inverted *Bsa*I restriction sites. The *B/c* cassette was excised from *Bsa*I-digested *pENTR-AtMIR390a-B/c*

(Addgene plasmid #51 778) [16] and ligated into *Bsa*I-digested *pENTR-BB* to generate *pENTR-B/c*. The *BB* cassette from *pENTR-BB* was transferred by LR recombination into *pMDC32B* [16] to generate *pMDC32B-BB*. Finally, the *B/c* cassette was excised from *Bsa*I-digested *pENTR-B/c* and ligated into *Bsa*I-digested *pMDC32B-BB* to generate *pMDC32B-B/c*. Oligonucleotides AC-1093/AC-1094 and AC-900/AC-901 including minimal *AtmiR173a TS* and *N. benthamiana NbmiR482a TS*-based precursors, respectively, were annealed and ligated into *Bsa*I-digested *pENTR-B/c* and *pMDC32B-B/c* to generate *pENTR-AtmiR173aTS-BB pENTR-NbmiR482aTS-BB*, *pMDC32B-AtmiR173aTS-BB*, and *pMDC32B-NbmiR482aTS-BB*, respectively. The B/c cassette was excised from *Bsa*I-digested *pENTR-AtTAS1c-D2-B/c* (Addgene plasmid #137 883) [18] and ligated into *Bsa*I-digested *pENTR-AtmiR173aTS-BB, pENTR-NbmiR482aTS-BB*, *pMDC32B-AtmiR173aTS-BB*, and *pMDC32B-NbmiR482aTS-BB* to generate *pENTR-AtmiR173aTS-B/c pENTR-NbmiR482aTS-B/c*, *pMDC32B-AtmiR173aTS-B/c*, and *pMDC32B-NbmiR482aTS-B/c*. New B/c vectors are available from Addgene: *pENTR-B/c* (Addgene plasmid #227 962), *pMDC32B-B/c* (Addgene plasmid #227 963), *pENTR-AtmiR173aTS-B/c* (Addgene plasmid #227 964), *pMDC32B-AtmiR173aTS-B/c* (Addgene plasmid #227 965), *pENTR-NbmiR482aTS-B/c* (Addgene plasmid #227 966), and *pMDC32B-NbmiR482aTS-B/c* (Addgene plasmid #227 967).

Oligonucleotide pairs AC-676/AC-677, AC-678/AC-679, AC-680/AC-681, AC-682/AC-683, AC-684/AC-685, AC-639/AC-640, AC-643/AC-644, AC-641/AC-642, and AC-645/AC-646 were annealed and ligated into *pENTR-D-TOPO* (Invitrogen) following manufacturer's instructions to generate *pENTR-min-GUS$_{At}$ pENTR-min-CH42*, *pENTR-min-FT*, *pENTR-min-FT/TRY*, *pENTR-min-TRY-FT*, *pENTR-min$_{482}$-GUS$_{Nb}$ pENTR-min$_{6019}$GUS$_{Nb}$ pENTR-min$_{482}$Su*, and *pENTR-min$_{6019}$-Su*, respectively. Minimal precursor cassettes were transferred by LR recombination into *pMDC32* [29] to generate *35S:min-GUS$_{At}$*, *35S:min-CH42*, *35S:min-FT*, *35S:min-FT-TRY*, *35S:min-TRY-FT*, *35S:min$_{482}$-GUS$_{Nb}$*, *35S:min$_{6019}$-GUS$_{Nb}$ 35S:min$_{482}$-Su*, and *35S: min$_{6019}$-Su*.

TS swaps were done by mutagenic polymerase chain reaction (PCR) using *pENTR:AtTAS1c-GUS$_{Nb}$* [17] as template and oligo pairs AC-631/AC-505 and AC-632/AC-507 to generate *pENTR-TAS$_{482}$-Su* and *pENTR-TAS$_{6019}$-Su*. *TAS1c*-based cassettes were transferred by LR recombination into *pMDC32* to generate *35S:TAS$_{482}$-Su* and *35S:TAS$_{6019}$-Su*.

Constructs *35S:min$_{156}$-Su*, *35S:min$_{173}$-Su*, and *35S:min$_{482}$-TSWV(x4)* were obtained by ligating annealed oligonucleotide pairs AC-719/AC-720–AC-721/AC-722 and AC-935/AC-936 into *pMDC32B-B/c* and *pMDC32B-NbmiR482aTS-B/c*, respectively, as described [16] (Supplementary Fig. S1 and S2). A detailed protocol for cloning syn-tasiRNA minimal precursors in B/c vectors is described in Supplementary Text S1.

For PVX-based amiRNA constructs, amiRNA cassettes *amiR-GUS$_{Nb}$* and *amiR-TSWV* were amplified from *35S:AtMIR390a-GUS$_{Nb}$* and *35S:AtMIR390a-TSWV-L-5* [20] with oligonucleotide pair AC-650/AC-663 and gel purified. For PVX-based syn-tasiRNA constructs, syn-tasiRNA cassettes *TAS$_{482}$-Su* and *min$_{482}$-TSWV(x4)* were amplified from *35S:TAS$_{482}$-Su* and *35S:min$_{482}$-TSWV(x4)* with oligonucleotide pairs AC-712/AC-713 and AC-988/AC-989 and gel purified. Syn-tasiRNA cassettes *min$_{482}$-Su* and *min$_{482}$-GUS$_{Nb}$(x4)* were ordered as dsDNA oligonucleotides AC-666 and AC-987. All amiRNA and syn-tasiRNA cassettes were assembled into *Mlu*I-digested and gel-purified *pLBPVXBa-M* (Addgene plasmid #229 079) [30] in the presence of GeneArt Gibson Assembly HiFi Master Mix (Invitrogen) to generate *35S:PVX-amiR-GUS$_{Nb}$*, *35S:PVX-amiR-TSWV*, *35S:PVX-min$_{482}$-Su*, *35S:PVX-min$_{482}$GUS$_{Nb}$(x4)*, and *35S:PVX-min$_{482}$-TSWV(x4)*. A detailed protocol for cloning syn-tasiRNA minimal precursors into *pLBPVXBa-M* is described in Supplementary Text S2. Syn-tasiRNA cassette min$_{482}$-Su was ordered as dsDNA oligonucleotide AC-667 and assembled into *Bsa*I-digested and gel-purified *pLX-TRV2* (Addgene plasmid #180 516) [31] in the presence of GeneArt Gibson Assembly HiFi Master Mix (Invitrogen) to generate *35S:TRV2-min482-Su*.

Syn-tasiRNA constructs *35S:TAS-GUS$_{At}$*, *35S:TAS-FT*, *35S:TAS-CH42*, *35S:TAS-FT-TRY*, *35S:TAS-TRY-FT*, *35S:TAS-GUS$_{Nb}$/MIR173*, *35S:TAS-Su/MIR173*, *35S:PVX*, *35S:TRV1*, and *35S:TRV2* constructs were described before [16, 18, 26, 31]. All DNA oligonucleotides used in this study are listed in Supplementary Table S1. The sequences of all syn-tasiRNA precursors are listed in Supplementary Text S3. The sequences of newly developed B/c vectors are listed in Supplementary Text S4. A detailed description of each construct functionally analysed *in vivo* is provided in Supplementary Table S2.

Transient expression of constructs and inoculation of viruses

Agrobacterium-mediated infiltration of DNA constructs in *N. benthamiana* leaves was done as previously [8, 32]. Preparation of crude extracts obtained from virus infected *N. benthamiana* plants was done as previously [26] with minor modifications. Briefly, all crude extracts were prepared by grinding infected tissue in a buffer containing 50 mM potassium phosphate (pH 8.0), 1% polyvinylpyrrolidone 10, and 1% polyethylene glycol 6000. Before inoculation, 5% silicon carbide (carborundum) was added to each crude extract. Syn-tasiRNA-based virus-induced gene silencing (syn-tasiR-VIGS) extracts were sprayed onto *N. benthamiana* leaves as previously described [26], while tomato spotted wilt virus (TSWV) extracts were mechanically inoculated by gently rubbing the leaf surface.

Chlorophyll extraction and analysis

Chlorophyll and other pigments from *N. bentamiana* leaves were extracted and analysed as described [18, 33].

RNA preparation

Total RNA form *N. benthamiana* leaves or from Arabidopsis seedlings or inflorescences was isolated as before [26]. Triplicate samples from pools of two *N. benthamiana* leaves or 9–12 Arabidopsis seedlings or inflorescences were analysed.

Real-time reverse transcription quantitative polymerase chain reaction (RT-qPCR)

Complementary DNA (cDNA) was obtained from 500 ng of DNAseI-treated total RNA from 10-day-old Arabidopsis seedlings, 60-day-old Arabidopsis plants, or from *N. benthamiana* leaves at 2 days post-agroinfiltration (dpa) using the

PrimeScript RT Reagent Kit (Perfect Real Time, Takara) according to manufacturer's instructions. Real time RT-qPCR was done using the same RNA samples that were used for sRNA-blot analysis. RT-qPCR was done on optical 96-well plates in a QuantStudio 3 Real-Time PCR system (Thermo Fisher Scientific, Waltham, MA, USA) using the following program: 20 s at 95°C, followed by 40 cycles of 95°C for 3 s, and 60°C for 30 s, with an additional melt curve stage consisting of 15 s at 95°C, 1 min at 60°C, and 15 s at 95°C. The 20-ml reaction mixture contained 10 ml of 2 × TB Green Premix Ex Taq (Takara), 2 ml of diluted complementary DNA (1:5), 0.4 ml of ROX II Reference Dye (50×f), and 300 nM of each gene-specific primer. Oligonucleotides used for RT-qPCR are listed in Supplementary Table S1. Target messenger RNA (mRNA) expression levels were calculated relative to reference genes *AtACT2* and *NbPP2A* in Arabidopsis and *N. benthamiana*, respectively, using the delta delta cycle threshold comparative method of QuantStudio Design and Analysis software, version 1.5.1 (Thermo Fisher Scientific). Three independent biological replicates, and two technical replicates for each biological replicate were analysed.

Stability and sequence analyses of syn-tasiRNA precursors during viral infections

Total RNA from apical leaves of each of the three biological replicates was pooled before cDNA synthesis. PCR to detect syn-tasiRNA precursors, PVX, and *NbPP2A* was performed using oligonucleotide pairs AC-654/AC-655, AC-657/AC-658, and AC-365/AC-366 (Supplementary Table S1), respectively, and Phusion DNA polymerase (Thermo Fisher Scientific). PCR products were analysed by agarose gel electrophoresis, and products of the expected sized were excised from the gel and sequenced when necessary.

Small RNA blot assays

Small RNA blot assays and band quantification from radioactive membranes were done as described [17]. Oligonucleotides used as probes for sRNA blots are listed in Supplementary Table S1.

Small RNA sequencing and data analysis

The quantity, purity, and integrity of total RNA was analysed with a 2100 Bioanalyser (RNA 6000 Nano kit, Agilent) and submitted to BGI (Hong Kong, China) for sRNA library construction and SE50 high-throughput sequencing in a DNBSEQ-G-400 sequencer. Quality-trimmed, adaptor removed clean reads received from BGI were used with the fastx_collapser toolkit (http:// hannonlab.cshl.edu/fastx toolkit) to collapse identical reads into a single sequence, while maintaining read counts. Mapping of each clean, unique read against the forward strand of the syn-tasiRNA precursor expressed in each sample (Supplementary Data S1) was done with a custom Python script not allowing mismatches or gaps, and also to calculate the counts and RPMs (reads per million mapped reads) for each mapping position. Processing accuracy of syn-tasiRNA precursors was assessed by quantifying the proportion of 19–24 nt sRNA (+) reads that mapped within ±4 nt of the 5′ end of the syn-tasiRNA guide as reported before [8, 33]. Phasing register tables were built by calculating the proportion of 21-nt sRNA (+) reads in each register relative to the corresponding amiRNA cleavage site for all 21-nt positions downstream of the cleavage site, as described previously [16].

Protein blot analysis

Proteins were separated in NuPAGE Novex 4%–12% Bis–Tris gels (Invitrogen), transferred to Protran nitrocellulose membranes (Amersham), and detected by chemiluminescence using specific antibodies and SuperSignal West Pico PLUS chemiluminescent substrate (Thermo Fisher Scientific). For detection of TSWV, anti-TSWV nucleocapsid (N) (Bioreba) was used at 1:10 000 dilution and conjugated with 1:20 000 of goat anti-rabbit IgG horseradish peroxidase secondary antibody (Thermo Fisher Scientific). Images were acquired with an ImageQuant 800 CCD imager (Cytiva) and analysed with ImageQuantTL v10.2 (Cytiva). Ponceau red S solution (Thermo Fisher Scientific) staining of membranes was used to verify the global protein content of the samples.

Statistical analysis

Statistical tests are described in the figure legends. Significant differences were determined with two-tailed Student's *t*-test.

Gene and virus identifiers

Arabidopsis and *N. benthamiana* gene identifiers are *AtACT2* (AT3G18780), *AtCH42* (AT4G18480), *AtFT* (AT1G65480), *AtTRY* (AT5G53200), *NbSu* (Nbv5.1tr6204879), and *NbPP2A* (Nbv5.1tr6224808), TSWV LL-N.05 segment L, M, and S genome identifiers are KP008128, FM163373, and KP008129, respectively. PVX-based constructs include PVX sequence variant MT799816.1. *Escherichia coli* β-glucuronidase gene sequence corresponds to GenBank accession number S69414.1.

Results

Effective gene silencing in *A. thaliana* by syn-tasiRNAs derived from minimal precursors

Previous work has shown that secondary siRNAs can be generated from non-*TAS* constructs including gene fragments fused to a 22-nt miRNA TS [14, 34]. Thus, we hypothesized that syn-tasiRNAs could similarly be produced from minimal precursors consisting exclusively of an endogenous 22-nt miRNA TS, followed by a 11-nt spacer fused to the syn-tasiRNA sequence. To test this, we used the syn-tasiR-FT/*AtFT* and syn-tasiR-CH42/*AtCH42* silencing sensor systems in Arabidopsis where transgenic expression of syn-tasiR-FT or syn-tasiR-CH42 from full-length *AtTAS1c* precursors at DCL4-processing position 3′D2[+] induces a significant delay in flowering time or an intense bleaching due to the targeting of *FLOWERING LOCUS T* (*AtFT*) or *CHLORINA 42* (*AtCH42*), respectively [18]. Here, we generated the *35S:min-FT* and *35S:min-CH42* constructs for expressing syn-tasiR-FT and syn-tasiR-CH42, respectively, from minimal precursors including exclusively the 22-nt (TS) sequence (GTGATTTTTCTCTACAAGCGAA) of Arabidopsis miR173a followed by the 11-nt spacer sequence (TAGACCATTTA) from *AtTAS1c* 3′D1[+] (Fig. 1A). The 11-nt spacer sequence from the endogenous *AtTAS1c* precursor of *A. thaliana* was selected because it has been previously used in multiple *AtTAS1c*-based constructs to successfully produce syn-tasiRNAs or secondary siRNAs in plants for efficient gene

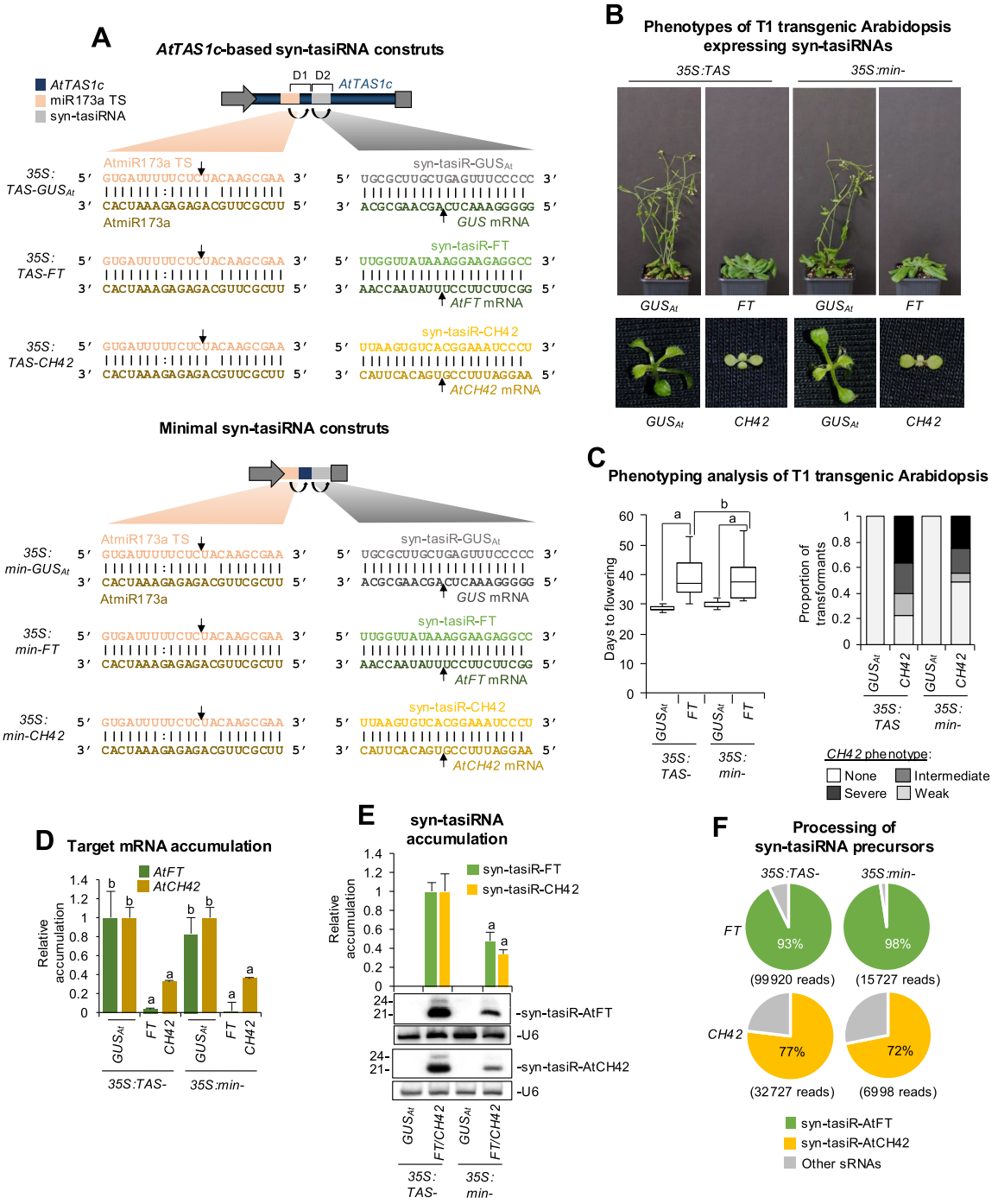

Figure 1. Functional analysis of *AtTAS1c* and minimal precursors expressing a single syn-tasiRNA against Arabidopsis *AtFT* or *AtCH42* in T1 transgenic plants. (**A**) Organization of syn-tasiRNA constructs. Diagram of *AtTAS1c* (up) and minimal (down) precursors including the AtmiR173a/AtmiR173a TS and syn-tasiRNA/target mRNA base-paring interactions. Arrows indicate the predicted cleavage sites for AtmiR173a and syn-tasiRNAs. (**B**) Representative photographs of Arabidopsis plants expressing syn-tasiRNAs from *AtTAS1c* or minimal precursors. Upper panel: 45-day-old plants expressing syn-tasiR-GUS_{At} or syn-tasiR-FT. Lower panel: 10-day-old seedlings expressing syn-tasiR-GUS_{At} or syn-tasiR-CH42. (**C**) Phenotypic analysis of plants expressing syn-tasiRNAs from *AtTAS1c* or minimal precursors. Left: Mean flowering time of plants expressing syn-tasiR-GUS_{At} or syn-tasiR-FT. Pairwise Student's *t*-test comparisons are represented with black lines including the letter 'a' if significantly different ($P < .05$) and the letter 'b' if not ($P > .05$). Right: Bar graphs representing, for each line, the proportion of seedlings displaying a severe (black areas), intermediate (dark grey areas), or weak (light grey areas) bleaching phenotype, or with wild-type appearance (white areas). (**D**) Target *AtFT* and *AtCH42* mRNA accumulation in RNA preparations from Arabidopsis plants [mean relative level ($n = 3$) + standard error] after normalization to *ACTIN 2*, as determined by quantitative RT-qPCR (*35S:TAS-*GUS_{At} = 1). Bars with the letter 'a' or 'b' are significantly different ($P < .05$) or not ($P > .05$) from the corresponding *35S:TAS1c-*GUS_{At} control samples, respectively, based on pairwise Student's *t*-test comparisons. (**E**) Northern blot detection of syn-tasiR-FT and syn-tasiR-CH42 in RNA preparations from Arabidopsis plants. The graph at the top shows the mean + standard deviation ($n = 3$) syn-tasiRNA relative accumulation (*35S:TAS1c-FT* = 1.0 and *35S:TAS-CH42* = 1.0). Bars with the letter 'a' are significantly different from that of *35S:TAS-FT* or *35S:TAS-CH42* control samples. One blot from three biological replicates is shown. Each biological replicate is a pool of at least nine independent lines selected randomly. U6 RNA blots are shown as loading controls. (**F**) Syn-tasiRNA processing from *AtTAS1c* or minimal precursors. Pie charts show the percentages of reads corresponding to the expected, accurately processed 21-nt mature syn-tasiR-FT and syn-tasiR-CH42 or to other 19–24-nt sRNAs (grey sectors).

silencing [14, 16, 18, 35–37]. In addition, the *35S:min-GUS$_{At}$* construct was also generated to express the syn-tasiR-GUS$_{At}$ syn-tasiRNA [24], targeting the *E. coli uidA* β-glucuronidase gene (or *GUS*), with no predicted off-targets in Arabidopsis and not inducing any noticeable phenotype, using a similar minimal precursor (Fig. 1A). These constructs were independently transformed into Arabidopsis Col-0 plants together with control constructs *35S:TAS-GUS$_{At}$*, *35S:TAS-FT* and *35S:TAS-CH42* expressing syn-tasiR-GUS$_{At}$, syn-tasiR-FT, and syn-tasiR-CH42, respectively, from position 3′D2[+] in *AtTAS1c*. These control constructs were previously shown to induce efficient target gene silencing [18]. To compare the activity of syn-tasiR-FT and syn-tasiR-CH42 produced from minimal and *AtTAS1c* precursors, plant phenotypes, syn-tasiRNA, and target mRNA accumulation as well as precursor processing efficiency were measured in Arabidopsis T1 transgenic lines.

All *35S:TAS-FT* ($n = 65$) and *35S:min-FT* ($n = 53$) transformants flowered later than the average flowering time of the *35S:TAS-GUS$_{At}$* and *35S:min-GUS$_{At}$* control lines ($n = 58$ and $n = 64$, respectively) (Fig. 1B and C and Supplementary Table S3). The average flowering time (39.3 ± 6.6 and 38.9 ± 6.6, respectively) was not significantly different between the two (Fig. 1C). RT-qPCR assays revealed that *FT* mRNA accumulation was similar in lines expressing syn-tasiR-FT from each of the two precursors (Fig. 1D), while RNA-blots showed that syn-tasiR-FT accumulated to significantly higher levels when expressed from full-length *AtTAS1c* precursors (Fig. 1E). Finally, high-throughput sequencing of sRNAs showed that *AtTAS1c* and minimal precursors were efficiently processed, with 93% and 98% of the reads corresponded to authentic syn-tasiR-FT, respectively (Fig. 1F). Similarly, all *35S:TAS-CH42* ($n = 402$) and *35S:min-CH42* ($n = 389$) transformants displayed bleaching to comparable degrees (Fig. 1B and C and Supplementary Table S4), accumulated similar levels of *AtCH42* mRNA (Fig. 1D) and displayed effective precursor processing (Fig. 1E and F), though reduced amounts of syn-tasiR-CH42 were observed in *35S:min-CH42* transformants (Fig. 1E).

Next, we analysed whether minimal precursors could be used to express multiple accurately processed and phased syn-tasiRNAs for the simultaneous silencing of different endogenous genes. For this purpose, we used the syn-tasiR-FT/syn-tasiR-TRY silencing sensor system in Arabidopsis, in which plants co-expressing both syn-tasiRNAs exhibit nonoverlapping silencing phenotypes of delay in flowering time and an increase in trichome number, due to the silencing of *AtFT* and of three *MYB* transcripts [*TRIPTYCHON (AtTRY)*, *CAPRICE* (*AtCPC*), and *ENHANCER OF TRIPTYCHON AND CAPRICE2 (AtETC2)*] [16] (Fig. 2A), respectively. Here, we compared the silencing efficacy of syn-tasiR-FT and syn-tasiR-TRY when co-expressed in unique dual configurations from positions 3′D2[+] and 3′D3[+] in full-length *AtTAS1c* (constructs *35S:TAS-FT-TRY* and *35S:TAS-TRY-FT*) or minimal precursors (constructs *35S:min-FT-TRY* and *35S:min-TRY-FT*) (Fig. 2B). We also included in the analysis control constructs *35S:TAS-GUS$_{At}$* and *35S:min-GUS$_{At}$* for expressing syn-tasiR-GUS$_{At}$ in single configuration from position 3′D2[+] in full-length *AtTAS1c* or minimal precursors, respectively. All these constructs were transformed into Arabidopsis Col-0 plants, and T1 transformants were analysed phenotypically by scoring the day of flowering and the trichome number in rosette leaves for each transformant, and molecularly by quantifying target mRNA and syn-tasiRNA accumulation in the different lines by RT-qPCR and RNA blot assays, respectively.

Regarding flowering time analysis, all transformants expressing the dual-configuration syn-tasiRNA constructs showed a delay in flowering compared to *35S:TAS-GUS$_{At}$* or *35S:min-GUS$_{At}$* control transformants (Fig. 2C and Supplementary Table S5). In particular, transformants expressing syn-tasiR-FT from minimal precursors at positions 3′D2[+] or 3′D3[+] had a mean flowering time of 43 ± 7.3 or 40.5 ± 5.4 days, respectively, which was similar to that of transformants expressing the same syn-tasiRNA from the same positions (43 ± 5.4 and 40.2 ± 3.9 days, respectively) (Fig. 2D). Regarding the trichome number analysis, 80% and 72% of transformants expressing syn-tasiR-TRY from minimal precursors at positions 3′D2[+] or 3′D3[+], respectively, had higher number of trichomes compared to the *35S:min-GUS$_{At}$* control group, similarly to the transformants expressing the same syn-tasiRNA from the same positions (88% and 82%, respectively) in full-length precursors (Supplementary Table S5). Interestingly, target mRNA accumulation analysis by RT-qPCR showed a similar and drastic decrease of *AtFT* and *AtTRY* mRNA levels in dual-configuration transformants compared to *35S:TAS-GUS$_{At}$* and *35S:min-GUS$_{At}$* controls, regardless of the size of precursor used (Fig. 2E). RNA blot assays confirmed that both minimal and full-length precursors produced detectable levels of syn-tasiRNAs (Fig. 2F). Notably, syn-tasiRNAs generated from the upstream D2[+] position accumulated at higher levels compared to those from the downstream D3[+] position. This increase was significant for syn-tasiRNAs derived from *AtTAS1c* precursors, as reported before [16, 18], but intriguingly, not for syn-tasiRNAs derived from minimal precursors. Importantly, syn-tasiRNAs accumulated as single 21-nt bands (Fig. 2F), suggesting an accurate processing from both types of precursors. To further confirm the accuracy of precursor processing, sRNAs from the four dual-configuration transformants were sequenced and analysed. Both classes of precursors were efficiently processed, with 95%–96% and 71%–89% of the reads corresponding to authentic syn-tasiR-FT or syn-tasiR-TRY, respectively (Fig. 2G). Moreover, the tasiRNA pools triggered by AtmiR173a were highly phased, with 93%–98% of 21-nt reads corresponding to the first register (Fig. 2G).

Overall, these results indicate that minimal syn-tasiRNA precursors, including the 22-nt AtmiR173a TS and the 11-nt *AtTAS1c* spacer, produce authentic 21-nt phased syn-tasiRNA species when stably expressed in Arabidopsis. These syn-tasiRNAs induce highly effective silencing of endogenous genes, similarly to those expressed from full-length *AtTAS1c* precursors.

Effective gene silencing in *N. benthamiana* by syn-tasiRNAs derived from minimal precursors

Next, we aimed to confirm in another plant species such as *N. benthamiana* that accurately processed and phased syn-tasiRNAs could be produced from minimal precursors. Since miR173a is exclusively present in Arabidopsis and its close relatives, we hypothesized that syn-tasiRNAs could be generated in *N. benthamiana* from minimal precursors including a TS from an endogenous 22-nt miRNA such as NbmiR482a or NbmiR6019a/b, instead of the original AtmiR173a TS.

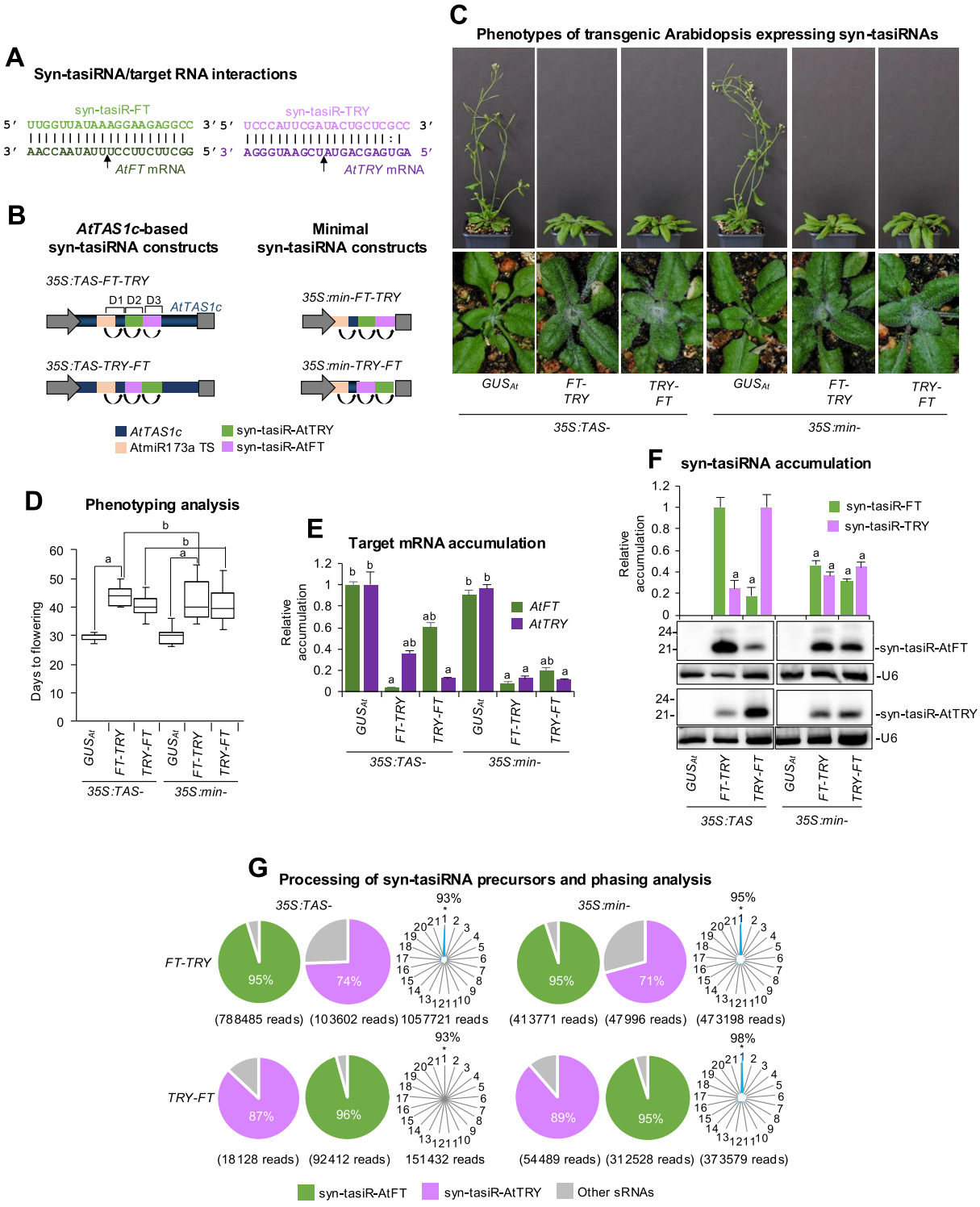

Figure 2. Functional analysis of *AtTAS1c* and minimal precursors expressing syn-tasiRNAs from distinct dual configurations in Arabidopsis T1 transgenic plants. (**A**) Base-pairing of syn-tasiRNAs and target mRNAs. Arrows indicate the syn-tasiRNA cleavage sites. (**B**) Diagram of *AtTAS1c* (left) and minimal (right) precursor constructs. Other details as in Fig. 1A. (**C**) Representative photographs of Arabidopsis plants expressing two syn-tasiRNAs in tandem from *TAS1c* or minimal precursors. The same plant was photographed at 20 days post-plating (dpp) to visualize the increased number of trichomes (bottom) and at 45 dpp to confirm the delay in flowering (top). (**D**) Phenotypic analysis of plants expressing syn-tasiRNAs from *AtTAS1c* or minimal precursors. Mean flowering time of plants expressing syn-tasiR-FT and syn-tasiR-TRY is represented. Other details as in Fig. 1C. (**E**) Target *AtFT* and *AtTRY* mRNA accumulation [mean relative level ($n = 3$) + standard error] after normalization to *ACTIN 2*, as determined by quantitative RT-qPCR (*35S:TAS-GUS*$_{At}$ = 1). Other details as in Fig. 1D. (**F**) Northern blot detection of syn-tasiR-FT and syn-tasiR-TRY in RNA preparations from Arabidopsis plants. The graph at the top shows the mean + standard deviation ($n = 3$) syn-tasiRNA relative accumulation (*35S:TAS-FT-TRY* and *35S:TAS-TRY-FT* = 1.0). Other details as in Fig. 1E. (**G**) Syn-tasiRNA processing and phasing analysis from *TAS1c*- and minimal precursors. Pie charts show the percentage of reads corresponding to expected, accurately processed 21-nt mature syn-tasiR-FT or syn-tasiR-TRY or to other 19–24 nt sRNAs. Radar plots show the proportion of 21-nt reads corresponding to each of the 21 registers from *AtTAS1c* transcripts, with position 1 designated as immediately after the AtmiR173a guided cleavage site. The percentage of 21-nt reads corresponding to phasing register 1 is indicated.

First, we examined whether syn-tasiRNA biogenesis could be triggered from the *35S:TAS$_{482}$-Su* or *35S:TAS$_{6019}$-Su* constructs engineered to produce syn-tasiR-Su, a syn-tasiRNA silencing the *N. benthamiana* magnesium chelatase subunit CHLI-encoding *SULPHUR* (*NbSu*) [17], from modified *AtTAS1c* precursors including NbmiR482a or NbmiR6019a/b TSs, respectively (Fig. 3A). Importantly, the accumulation of syn-tasiR-Su in *N. benthamiana* leaves induces strong bleaching [17, 18], making this system a convenient model for studying syn-tasiRNA biogenesis and facilitating the visual observation of target gene silencing. Both constructs were independently agroinfiltrated in two areas of two leaves from three different plants, together with control constructs *35S:TAS-Su/MIR173* and *35S:TAS-GUS$_{Nb}$/MIR173*. These constructs were expected to produce syn-tasiR-Su and syn-tasiR-GUS$_{Nb}$—a syn-tasiRNA targeting GUS with no off-targets in *N. benthamiana* [17]—respectively, due to the co-expression of AtmiR173a from the *MIR173a* precursor included within the same construct (Fig. 3A) [18]. At 7 dpa, all areas agroinfiltrated with anti-*NbSu* syn-tasiRNA constructs displayed a strong bleaching, as expected from *NbSu* knockdown, while areas expressing the control syn-tasiRNA did not (Fig. 3A). These bleached areas accumulated significantly reduced amounts of chlorophyll *a* compared to areas expressing the control syn-tasiRNA (Fig. 3B). Next, two leaves of three different plants were independently agroinfiltrated over the entire leaf surface with each of the syn-tasiRNA constructs described above. RT-qPCR and RNA blot assays of RNA preparations obtained at 2 dpa from agroinfiltrated leaves showed that, in all samples expressing canonical or modified *AtTAS1c* precursors, *NbSu* mRNA accumulation was drastically reduced and syn-tasiR-Su accumulated as a single 21-nt band, although samples expressing *TAS$_{6019}$-Su* accumulated lower levels of syn-tasiR-Su than the others (Fig. 3C and D). Importantly, high-throughput sequencing analysis of sRNAs showed that *TAS$_{482}$* and canonical *AtTAS1c* precursors were processed with similar accuracy, with 59% and 58% of reads within ±4 nt of 3′D2[+] corresponded to authentic syn-tasiR-Su, respectively, while this percentage was lower (37%) in samples expressing *TAS$_{6019}$* precursors (Fig. 3E). Moreover, highly phased siRNAs were generated from canonical *TAS1c* or modified *TAS$_{482}$* precursors, with 63% and 54% of 21-nt [+] reads, respectively, corresponding to the first register (Fig. 3E). In the case of *TAS$_{6019}$* precursors, only 39% of 21-nt [+] reads corresponded to the first register (Fig. 3E).

Next, we decided to test whether syn-tasiRNA biogenesis could be triggered in *N. benthamiana* from the *35S:min$_{482}$-Su* and *35S:min$_{6019}$-Su* constructs engineered for syn-tasiR-Su expression from minimal precursors including miR482a or miR6019a/b TS, respectively (Fig. 4A). Both constructs were agroinfiltrated in *N. benthamiana* and analysed as explained before together with *35S:TAS-GUS$_{Nb}$/MIR173a*, *35S:TAS$_{482}$-Su*, and *35S:TAS$_{6019}$-Su* (Fig. 4A), analysed in parallel for comparative purposes (Fig. 4A). All constructs engineered for expressing syn-tasiR-Su induced bleaching in the agroinfiltrated areas (Fig. 4A), which correlated with drastic *NbSu* mRNA downregulation compared to the negative control samples (Fig. 4B). RNA blot assays confirmed the accumulation of syn-tasiR-Su as a single 21-nt sRNA species in all samples displaying bleaching, with samples expressing *min$_{482}$*precursors accumulating syn-tasiRNAs to levels similar to those of samples expressing *TAS$_{482}$* precursors (Fig. 4C). Moreover, the *min$_{482}$* precursor was efficiently processed, as 63% of ±4 nt of 3′D2[+] reads corresponded to authentic syn-tasiR-Su. This percentage was similar to that of full-length *AtTAS1c* precursor (58%, Fig. 3E) and slightly higher than that of the *min$_{6019}$* precursor (Fig. 4D).

Finally, to confirm that syn-tasiRNA biogenesis from minimal precursors in *N. benthamiana* requires an endogenous 22-nt miRNA, leaves agroinfiltrated with the *35S:min$_{156}$-Su* and *35S:min$_{173}$-Su* constructs were analysed. These constructs were engineered for expressing syn-tasiR-Su from minimal precursors including either a *N. benthamiana* 21-nt miRNA (NbmiR156a) TS or a heterologous 22-nt miRNA (AtmiR173a) TS, respectively (Supplementary Fig. S3A). Results show that leaves agroinfiltrated with either of these two constructs displayed neither bleaching (Supplementary Fig. S3A) nor reduced chlorophyll *a* content (Supplementary Fig. S3B), nor accumulation of syn-tasiR-Su (Supplementary Fig. S3C). These results also suggest that bleaching observed in leaves agroinfiltrated with *35S:min$_{482}$-Su* is due to the activity of syn-tasiR-Su rather than of potential siRNAs generated from transgene silencing. Taken together, all these findings demonstrate that highly phased, accurately processed syn-tasiRNAs can be produced in *N. benthamiana* from minimal precursors including a heterologous TS from an endogenous 22-nt miRNA.

Widespread gene silencing in *N. benthamiana* triggered by syn-tasiRNAs derived from minimal precursors and expressed from a viral vector

The use of viral vectors to express syn-tasiRNAs for silencing plant genes has not been reported. Here, we tested this possibility and hypothesized that the 54-nt long *min$_{482}$*-based precursor (when including a single syn-tasiRNA) could be more stable when inserted in a viral vector than the classic, 1011-nt long *TAS$_{482}$*-based precursor. Minimal precursors including NbmiR482a TS were more accurately processed and produced increased syn-tasiRNA accumulation compared to NbmiR6019a/b TS (Fig. 4C and D) most likely due to higher NbmiR482 abundance compared to precursors including NbmiR6019a/b TS (Supplementary Fig. S4). Thus, precursors including NbmiR482a TS were preferred and analysed in further experiments.

To analyse syn-tasiRNA biogenesis from a viral vector, *TAS$_{482}$-Su* and *min$_{482}$-Su* sequences were inserted into a potato virus X (PVX) infectious clone to generate the *35S:PVX-TAS$_{482}$-Su* and *35S:PVX-min$_{482}$-Su* constructs, respectively (Fig. 5A). Both constructs were expected to express syn-tasiR-Su from full-length *TAS$_{482}$* and minimal *min$_{482}$* precursors, respectively, during PVX infection and induce bleaching of PVX-infected tissues. These two constructs, along with the insert-free *35S:PVX* construct, which was not expected to induce any bleaching (Fig. 5A), were independently agroinoculated into one leaf of three *N. benthamiana* plants. A negative control set of plants (‘mock’) was infiltrated with agroinfiltration solution. The appearance of mild PVX-induced symptoms and bleaching silencing phenotypes were monitored during 28 dpa.

All plants agroinoculated with *35S:PVX* or *35S:PVX-min$_{482}$-Su* showed mild leaf curling typical of PVX-induced symptoms between 4 and 5 dpa (Fig. 5B). In contrast, plants agroinoculated with *35S:PVX-TAS$_{482}$-Su* displayed the curling phenotype 2–3 days later, between 7 and 8 dpa (Fig. 5B). Interestingly, bleaching was observed in areas of certain

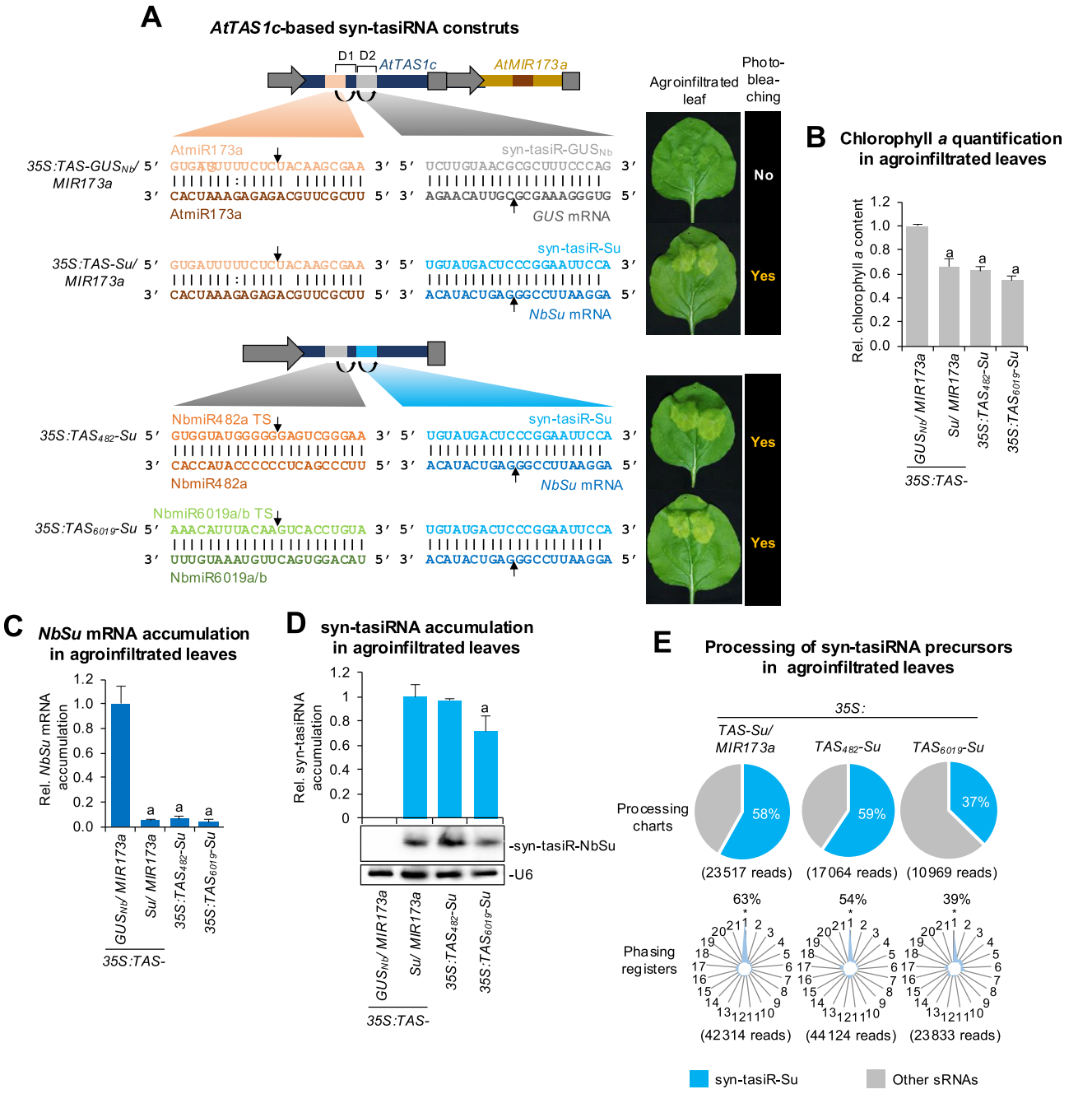

Figure 3. Functional analysis of syn-tasiRNAs against *N. benthamiana SULPHUR* (*NbSu*) expressed from modified *AtTAS1c* precursors including endogenous 22-nt miRNA TS. (**A**) Organization of *AtTAS1c*-based syn-tasiRNA constructs. Left: Upper section shows constructs with canonical *AtTAS1c* precursors for expressing syn-tasiR-GUS_{Nb} or syn-tasiR-Su together with AtmiR173a; lower section shows constructs with modified *AtTAS1c* precursors including NbmiR482a or NbmiR6019a/b TS. Other details as in Fig. 1A. Right: Photographs at 7 days post agroinfiltration (dpa) of leaves agroinfiltrated with each of construct. The presence or absence of bleaching on the agroinfiltrated patches is labelled as 'Yes' or 'No', respectively. (**B**) Relative content of chlorophyll *a* in agroinfiltrated patches (*35S:TAS-*GUS_{Nb}*/MIR173a* = 1.0). Bars with letter 'a' are significantly different from the control sample ($P <$ .05 in pairwise Student's *t*-test comparisons). (**C**) Target *NbSu* mRNA accumulation in agroinfiltrated leaves at 2 dpa [mean relative level ($n = 3$) + standard error] after normalization to *PROTEIN PHOSPHATASE 2A* (*PP2A*), as determined by quantitative RT-qPCR (*35S:TAS-*GUS_{Nb}*/MIR173a* = 1). Other details are as in panel (B). (**D**) Northern blot detection of syn-tasiR-NbSu in RNA preparations from agroinfiltrated leaves at 2 dpa. The graph at top shows the mean + standard deviation ($n = 3$) syn-tasiRNA relative accumulation (*35S:TAS-Su/MIR173a* = 1.0). Other details are as in Fig. 1E. (**E**) Syn-tasiRNA processing and phasing analysis from *TAS1c*-derived precursors. Pie charts show the percentages of reads corresponding to expected, accurately processed 21-nt mature syn-tasiR-Su or to other 19–24 nt sRNAs. Radar plots show the proportion of 21-nt reads corresponding to each of the 21 registers from *AtTAS1c* transcripts, with position 1 designated as immediately after AtmiR173a, NbmiR482a, or NbmiR6019a/b guided cleavage site.

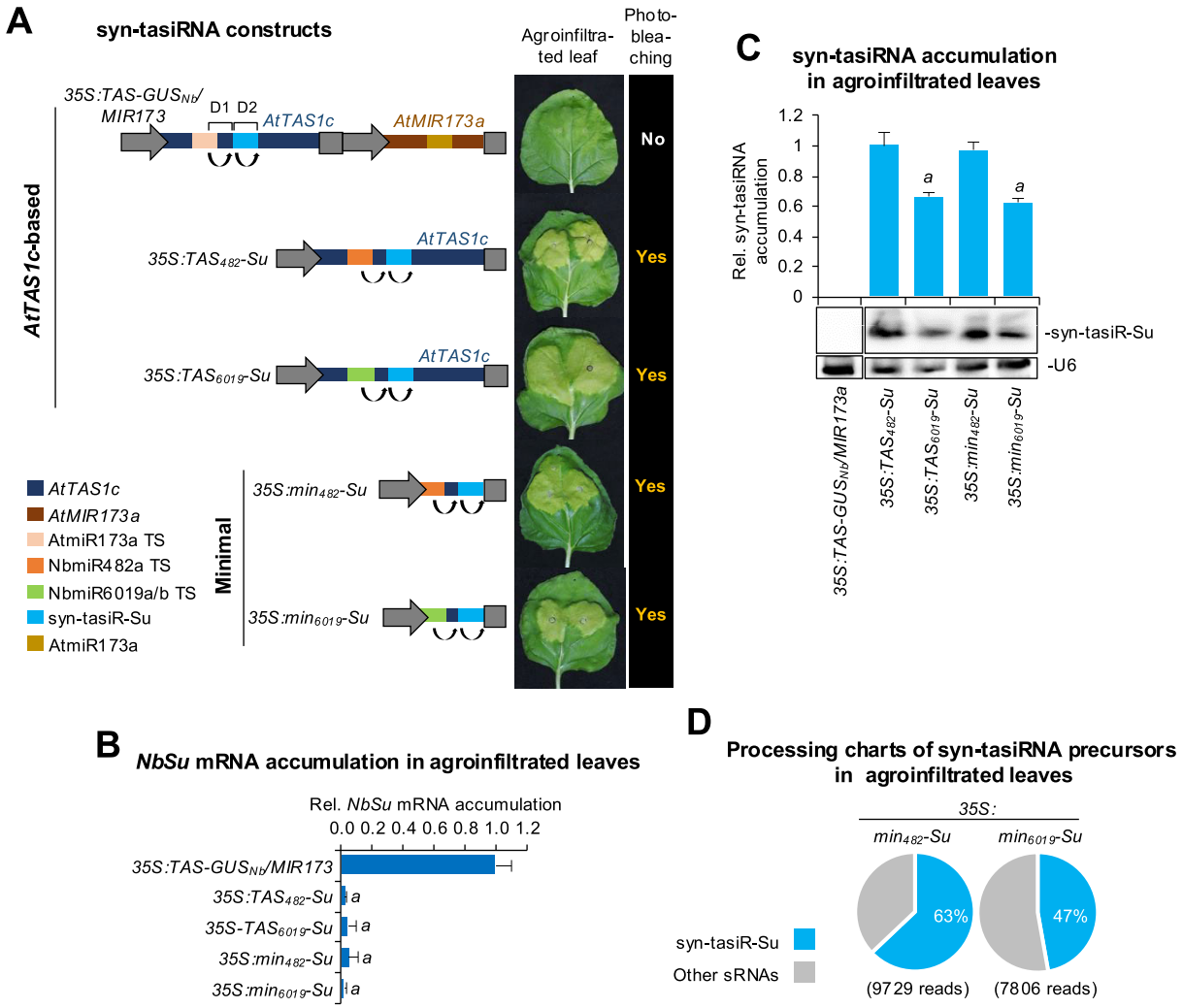

Figure 4. Functional analysis in *N. benthamiana* leaves of syn-tasiR-Su expressed from minimal precursors including NbmiR482a or NbmiR6019a/b TS. (**A**) Diagram of *AtTAS1c*-based or minimal precursor constructs. Other details as in Fig. 3A. (**B**) Target *NbSu* mRNA accumulation in agroinfiltrated leaves at 2 days post-agroinfiltration (dpa) [mean relative level ($n = 3$) + standard error] after normalization to *PROTEIN PHOSPHATASE 2A* (*NbPP2A*), as determined by RT-qPCR. Other details are as in Fig. 3B. (**C**) Northern blot detection of syn-tasiR-Su in RNA preparations from agroinfiltrated leaves at 2 dpa. The graph at top shows the mean + standard deviation ($n = 3$) syn-tasiRNA relative accumulation [*35S:TAS*$_{482}$*-Su* = 1.0]. Other details are as in Fig. 1E. (**D**) Syn-tasiRNA processing from minimal precursors. Pie charts show the percentages of reads corresponding to expected, accurately processed 21-nt mature syn-tasiR-Su or to other 19–24 nt sRNAs.

apical leaves as soon as 7 dpa in plants agroinoculated with *35S:PVX-min*$_{482}$*-Su*, and by 14–21 dpa it extended to most of the apical tissues (Fig. 5C). At these same timepoints, limited and mild bleaching was observed in plants agroinoculated with *35S:PVX-TAS*$_{482}$*-Su* while no bleaching was observed in plants expressing *35S:PVX* (Fig. 5C). RT-qPCR and RNA blot analyses showed that only tissues expressing *35S:PVX-min*$_{482}$*-Su* accumulated low levels of *NbSu* mRNA (Fig. 5D) and high levels of syn-tasiR-Su, respectively (Fig. 5E). In contrast, plants agroinoculated with *35S:PVX-TAS*$_{482}$*-Su* displayed a slight decrease in *NbSu* mRNA levels and low levels of syn-tasiR-NbSu barely detectable by RNA blot assay (Fig. 5E). Importantly, sRNA sequencing of RNA preparations from apical leaves of plants agroinoculated with *35S:PVX-min*$_{482}$*-Su* revealed that the *min*$_{482}$*-Su* precursor was accurately processed, with 55% of the ±4 nt of 3′D2[+] reads corresponding to authentic syn-tasiR-Su (Fig. 5F). Plotting all 19–24-nt sRNA [+] reads that map to the whole *35S:PVX-min*$_{482}$*-Su* precursor revealed a relatively low number of sRNAs overlapping with the 3′D2[+] position or, more generally, produced from the rest of the precursor (Fig. 5F). Indeed, the sRNA profile of 19–24-nt [+] reads mapping to the *min*$_{482}$*-Su* precursor was similar in *35S:PVX-min*$_{482}$*-Su* and *35S:min*$_{482}$*-Su* samples thus indicating that processing of the minimal precursor is not particularly altered during PVX replication (Supplementary Fig. S5). Finally, the presence of *TAS*$_{482}$*-Su* and *min*$_{482}$*-Su* precursors was analysed by RT-PCR at 7 dpa with oligonucleotides flanking the precursor insertion site. The 278-bp fragment corresponding to the *min*$_{482}$*-Su* precursors was clearly amplified while the 1235-bp fragment of the *TAS*$_{482}$*-Su* could not be detected. PVX coat protein (CP) was detected in all samples expressing PVX-based constructs, and *NbPP2A* in all samples, thus excluding the possibility that the absence of *TAS*$_{482}$*-Su* precursors was due to either a lack of infection in these samples or deficient cDNA synthesis. Sanger sequencing of RT-PCR fragments amplified from the three *PVX-min*$_{482}$*-Su*-infected samples revealed no mutations in the whole insert.

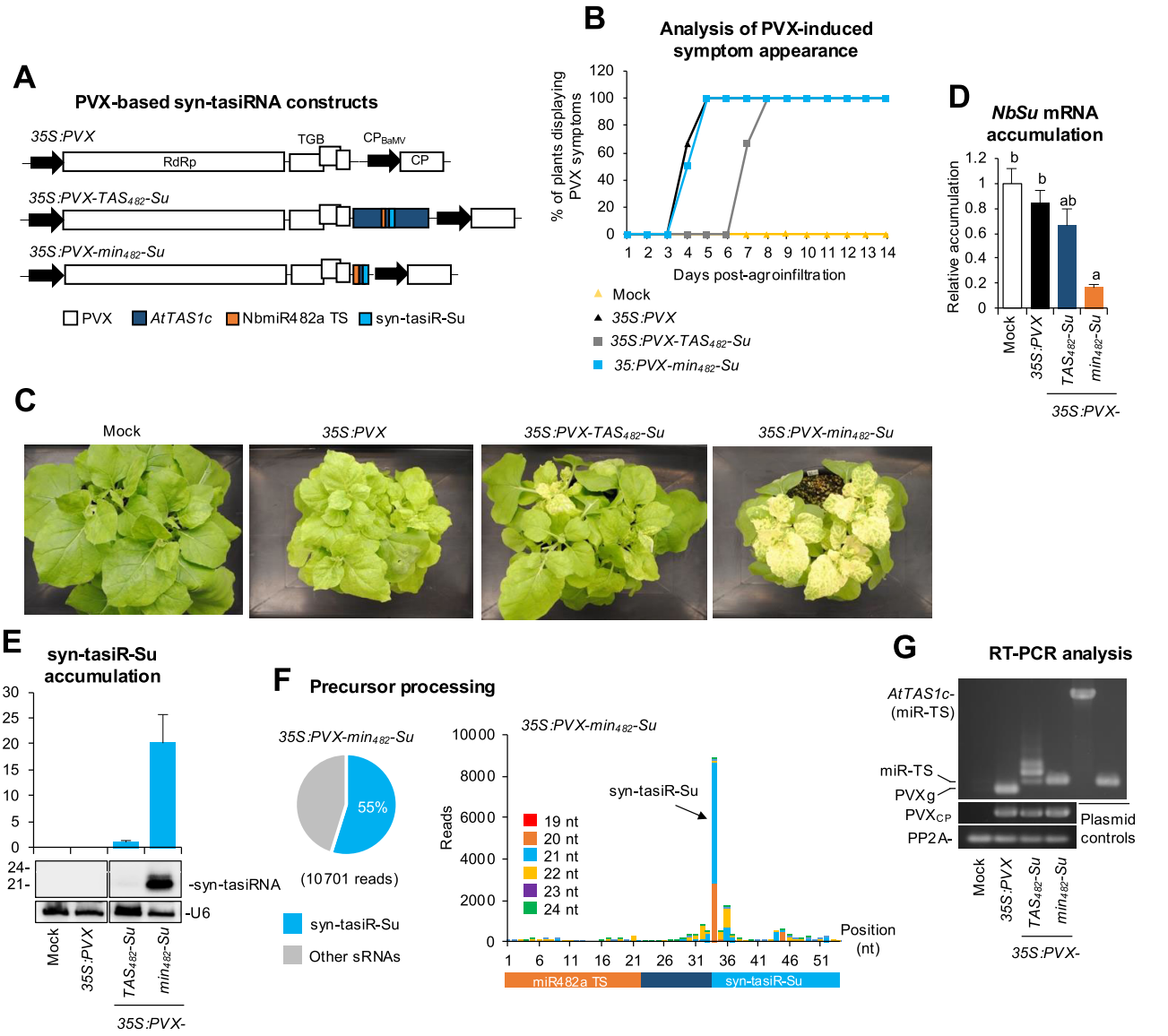

Figure 5. Functional analysis of PVX constructs expressing syn-tasiR-Su from *AtTAS1c* or minimal syn-tasiRNA precursors in *N. benthamiana*. (**A**) Diagram of PVX-based constructs. PVX open reading frames (ORFs) and promoters are represented as boxes and arrows, respectively. RdRP, RNA-dependent RNA-polymerase; TGB, triple gene block; CP, coat protein; CP_{BaMV}, Bamboo mosaic virus CP promoter. (**B**) Two-dimensional line graph showing, for each of the three-plant sets listed, the percentage of symptomatic plants per day during 14 days. (**C**) Photos at 14 days post-agroinfiltration (dpa) of sets of three plants agroinoculated with the different constructs. (**D**) Target *NbSu* mRNA accumulation in RNA preparations from apical leaves collected at 14 dpa and analysed individually (mock = 1.0 in all comparisons). Bars with the letter 'a' or 'b' indicate whether the mean values are significantly different from mock control or *35S:PVX-min*$_{482}$*-Su* samples, respectively ($P < .05$ in pairwise Student's *t*-test comparison). (**E**) Northern blot detection of syn-tasiR-Su in RNA preparations from apical leaves collected at 14 dpa and pooled from three independent plants. The graph at the top shows the mean + standard deviation ($n = 3$) syn-tasiRNA relative accumulation [*35S:TAS*$_{482}$*-Su* = 1.0]. (**F**) syn-tasiRNA processing from *PVX-min*$_{482}$*-Su*. Left: Pie chart shows the percentage of reads corresponding to expected, accurately processed 21-nt mature syn-tasiR-Su or to other 19–24 nt sRNAs. Right: sRNA profile of 19–24 nt [+] reads mapping to each of the 54 nucleotide positions in the *min*$_{482}$*-Su* precursor from samples expressing *35S:PVX-min*$_{482}$*-Su*. (**G**) Reverse transcriptase-polymerase chain reaction (RT-PCR) detection of PVX, *AtTAS1c*, and minimal precursors in apical leaves at 7 dpa. RT-PCR products corresponding to the *NbPP2A* and PVX vector controls are also shown (bottom), as well as control amplifications of *AtTAS1c* and minimal precursor fragments from plasmids (right). PVXg, band amplified from *35S:PVX* samples corresponding to the genomic region lacking a syn-tasiRNA precursor.

Importantly, to further confirm that *NbSu* silencing was due to syn-tasiR-Su activity and not to potential siRNAs generated from the *min*$_{482}$*-Su* precursor during PVX replication, a set of three plants were agroinoculated with the *35S:PVX-min*$_{173}$*-Su* construct (Supplementary Fig. S6A). As controls, sets of three plants were also mock-inoculated, or agroinoculated with the *35S:PVX* or *35S:PVX-min*$_{482}$*-Su* constructs. At 14 dpa, plants agroinoculated with the *35S:PVX-min*$_{173}$*-Su* construct did not display any bleaching (Supplementary Fig. S6B) or reduced *NbSu* mRNA levels (Supplementary Fig. S6C). These plants did not accumulate syn-tasiR-Su (Supplementary Fig. S6D), although they did accumulate PVX variants containing the *min*$_{173}$*-Su* precursors (Supplementary Fig. S6D). Overall, these results demonstrate that accurately processed syn-

tasiRNAs can be produced from minimal precursors inserted into PVX, enabling widespread silencing of endogenous plant genes such as *NbSu*.

Because PVX induces mild but clearly visible symptoms in *N. benthamiana* (Fig. 5C), we evaluated whether syn-tasiR-VIGS could be triggered by an asymptomatic viral vector, such as tobacco rattle virus (TRV) [38]. To this end, the *min$_{482}$-Su* sequence was inserted in a TRV infectious clone to generate the *35S:TRV2-min$_{482}$-Su* construct (Supplementary Fig. S7A). This construct, along with the insert-free 35S:*TRV2* control construct, was independently agroinoculated into a single leaf of three *N. benthamiana* plants. Importantly, in both cases, the 35S*:TRV1* construct was co-infiltrated to facilitate TRV infection [31]. As before, a negative control ('mock') group of plants was infiltrated with agroinfiltration solution. At 14 dpa. strong bleaching covering most of the apical tissue surface was observed in all plants agroinoculated with the *35S:TRV2-min$_{482}$-Su* construct, but not in the control plants (Supplementary Fig. S7B). At this same time point, plants agroinoculated with the empty-free *35S:TRV2* construct did not exhibit any virus-induced symptoms, as reported before [38]. RT-qPCR analysis revealed that only tissues from plants agroinoculated with *35S:TRV2-min$_{482}$-Su* accumulated low levels of *NbSu* mRNA (Supplementary Fig. S7C). Finally, RT-PCR analysis at 7 dpa confirmed the presence of the *min$_{482}$-Su* precursor band, while TRV was detected in all samples expressing TRV-based constructs, and *NbPP2A* was detected in all samples (Supplementary Fig. S7D). Taken together, these results show that syn-tasiR-VIGS can be efficiently triggered in *N. benthamiana* using a symptomless viral vector such as TRV.

Plant immunization against a pathogenic virus with antiviral syn-tasiRNAs produced from the PVX viral vector

Previous work showed that transgenically expressed syn-tasiRNAs induce enhanced antiviral resistance compared to amiRNAs due to the combined silencing effect of each individual syn-tasiRNA [37]. Here, we explored the possibility of using syn-tasiR-VIGS to induce antiviral resistance against TSWV, an economically important plant pathogen affecting different crops worldwide [39], in *N. benthamiana*. To this end, we generated the *35S:PVX-min$_{482}$-TSWV(x4)* construct, which includes the 22-nt TS of miR482a followed by the 11-nt *AtTAS1c* spacer and four different 21-nt syn-tasiRNA sequences (syn-tasiR-TSWV-1, syn-tasiR-TSWV-2, syn-tasiR-TSWV-3, and syn-tasiR-TSWV-4) (Fig. 6A) with known anti-TSWV activity [20]. A similar construct named *35S:PVX-min$_{482}$-GUS$_{Nb}$(x4)*, expected to produce four innocuous anti-GUS syn-tasiRNAs (syn-tasiR-GUS$_{Nb}$ and syn-tasiR-GUS$_{Nb}$-2) of different sequences, was also generated (Fig. 6A). Additionally, the *35S:PVX-amiR-GUS$_{Nb}$* and *35S:PVX-amiR-TSWV* constructs, expected to produce amiR-GUS$_{Nb}$ and amiR-TSWV amiRNAs [20] (which have identical sequences to syn-tasiR-GUS$_{Nb}$ and syn-tasiR-TSWV-1, respectively) were generated for comparative purposes (Fig. 6A). These constructs were agroinoculated into one leaf of nine *N. benthamiana* plants, six of which were mechanically inoculated seven days later with a TSWV infectious extract. An additional set of mock-inoculated plants was also included. To determine the antiviral activity of art-sRNAs, the appearance of typical TSWV-induced symptoms (leaf epinasty and chlorosis) in apical noninoculated tissues was monitored over 21 days post-inoculation (dpi), and the presence of PVX and TSWV by RT-PCR or western blot.

None of the plants agroinoculated with the *35S:PVX-min$_{482}$-TSWV(x4)* construct displayed typical TSWV-induced symptoms throughout the experiment, while plants expressing *35S:PVX-amiR-TSWV* became symptomatic, although with a significant 1–6-day delay compared to plants agroinoculated with control constructs (Fig. 6B and C). At 14 dpi, TSWV was undetectable in protein extracts from plants agroinoculated with *35S:PVX-min$_{482}$-TSWV(x4)*, while high or low levels of TSWV were detected in control and amiR-TSWV-expressing plants, respectively (Fig. 6D). Importantly, PVX variants including the corresponding art-sRNA precursor were detected by RT-PCR, indicating that the lack of protection was not due to the lack of PVX infection or the loss of the art-sRNA precursor (Fig. 6E). Finally, northern blot analysis confirmed art-sRNA accumulation in plants agroinoculated with PVX-based constructs, with both amiR-TSWV and anti-TSWV syn-tasiRNAs accumulating predominantly as 21-nt sRNA species (Fig. 6F). The accuracy of *min$_{482}$-TSWV(x4)* precursor processing and the production of authentic anti-TSWV syn-tasiRNAs were analysed by high-throughput sequencing of sRNA libraries from plants agroinoculated with *35S:PVX-min$_{482}$-TSWV(x4)* (Fig. 6G). All four syn-tasiRNA sequences were detected as predominant when plotting all 19–24-nt sRNA [+] reads mapping to the precursor, with 66%, 85%, 31%, and 13% of reads within ±4 nt of 3′D2 [+], 3′D3 [+], 3′D4 [+], and 3′D5 [+], respectively, corresponded to authentic syn-tasiRNAs (Fig. 6G). Additionally, highly phased syn-tasiRNAs were generated, with 63% of 21-nt [+] reads corresponding to the first register (Fig. 6G). Taken together, these findings indicate that PVX-based syn-tasiR-VIGS can be used to vaccinate plants against TSWV for complete immunization. They also highlight that multiple syn-tasiRNAs can be produced simultaneously *in planta* from an RNA viral vector such as PVX.

Transgene-free, PVX-based syn-tasiR-VIGS

We finally explored the possibility of applying syn-tasiR-VIGS to plants in a DNA-free, nontransgenic manner for both silencing endogenous genes or for plant antiviral vaccination (Fig. 7A). To do so, six *N. benthamiana* plants were independently agroinoculated with either *35S:PVX*, *35S:PVX-min$_{482}$-Su*, *35S:PVX-min$_{482}$-GUS$_{Nb}$(x4)*, or *35S:PVX-min$_{482}$-TSWV(x4)*. At 6 dpa, apical leaves displaying mild PVX-induced symptoms were collected together and a crude extract was prepared for each case (Fig. 7A).

First, crude extracts including PVX-min$_{482}$-Su were sprayed onto three *N. benthamiana* plants and the appearance of bleaching was monitored over 14 days (Fig. 7A). Control crude extracts from mock- and empty PVX-agroinoculated plants were sprayed in parallel. Remarkably, all three *N. benthamiana* plants sprayed with crude extracts derived from *35S:PVX-min$_{482}$-Su* displayed bleaching indicative of *NbSu* silencing (Fig. 7B) and accumulated minimal syn-tasiRNA precursors (Fig. 7C), with no sequence alterations as confirmed by Sanger sequencing of RT-PCR products. Control plants sprayed with empty extracts displayed mild PVX symptoms but no bleaching and accumulated PVX RNAs, while plants sprayed with mock extracts were symptomless as well as bleaching- and virus-free (Fig. 7B and C).

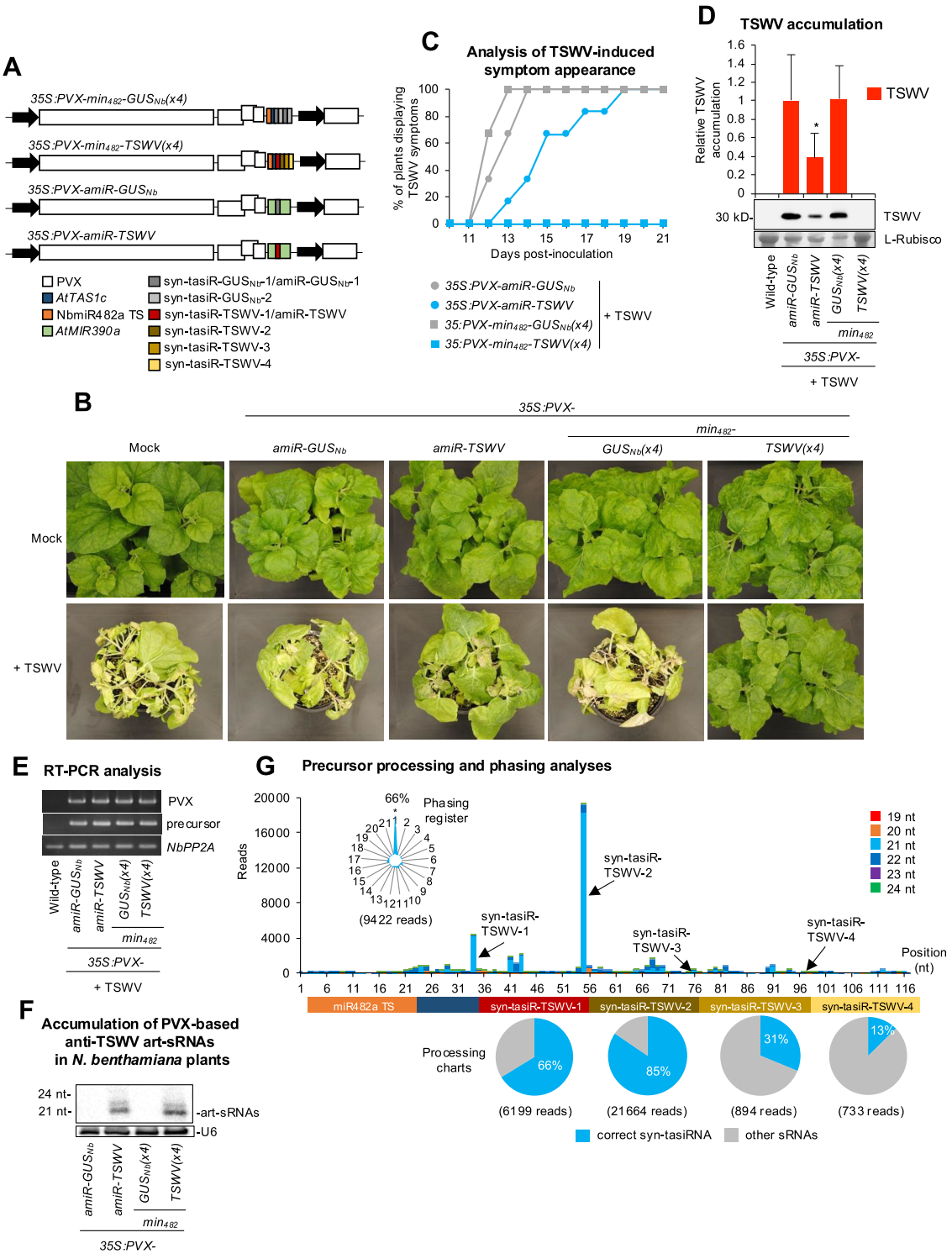

Figure 6. Functional analysis of PVX constructs expressing syn-tasiRNAs against TSWV in *N. benthamiana*. (**A**) Diagram of PVX-based constructs. Other details are as in Fig. 5A. (**B**) Photos at 21 days post-inoculation (dpi) of sets of three plants agroinoculated with the different constructs and inoculated or not (mock) with TSWV. (**C**) Two-dimensional line graph showing, for each of the six-plant sets listed, the percentage of symptomatic plants per day during 21 days. (**D**) Western blot detection of TSWV in protein preparations from apical leaves collected at 14 dpi and pooled from six independent plants. The graph at top shows the mean + standard deviation ($n = 6$) TSWV relative accumulation [*35S:PVX-amiR-GUS*$_{Nb}$ = 1.0]. Bars with the letter 'a' are significantly different from that of *35S:PVX-amiR-GUS*$_{Nb}$ control sample ($P < .05$ in pairwise Student's *t*-test comparison). The membrane stained with Ponceau red showing the large subunit of Rubisco (ribulose1,5-biphosphate carboxylase/oxygenase) is included as loading control. (**E**) RT-PCR detection of PVX and minimal precursors in apical leaves at 7 dpa. RT-PCR products corresponding to the *NbPP2A* and PVX vector controls are also shown (bottom). (**F**) Northern blot detection of anti-TSWV art-sRNAs in RNA preparations from apical leaves collected at 7 dpa and pooled from three independent mock-inoculated plants. (**G**) syn-tasiRNA processing from *PVX-min*$_{482}$*-TSWV(x4)*. Top: sRNA profile of 19–24 nt [+] reads mapping to each of the 117 nucleotide positions in the *min*$_{482}$*-TSWV(x4)* precursor from samples expressing *35S:PVX-min*$_{482}$*-TSWV(x4)*. Other details are as in panel (A). Bottom: Pie charts showing the percentages of reads corresponding to expected, accurately processed 21-nt mature forms of each of the four anti-TSWV syn-tasiRNAs or to other 19–24 nt sRNAs.

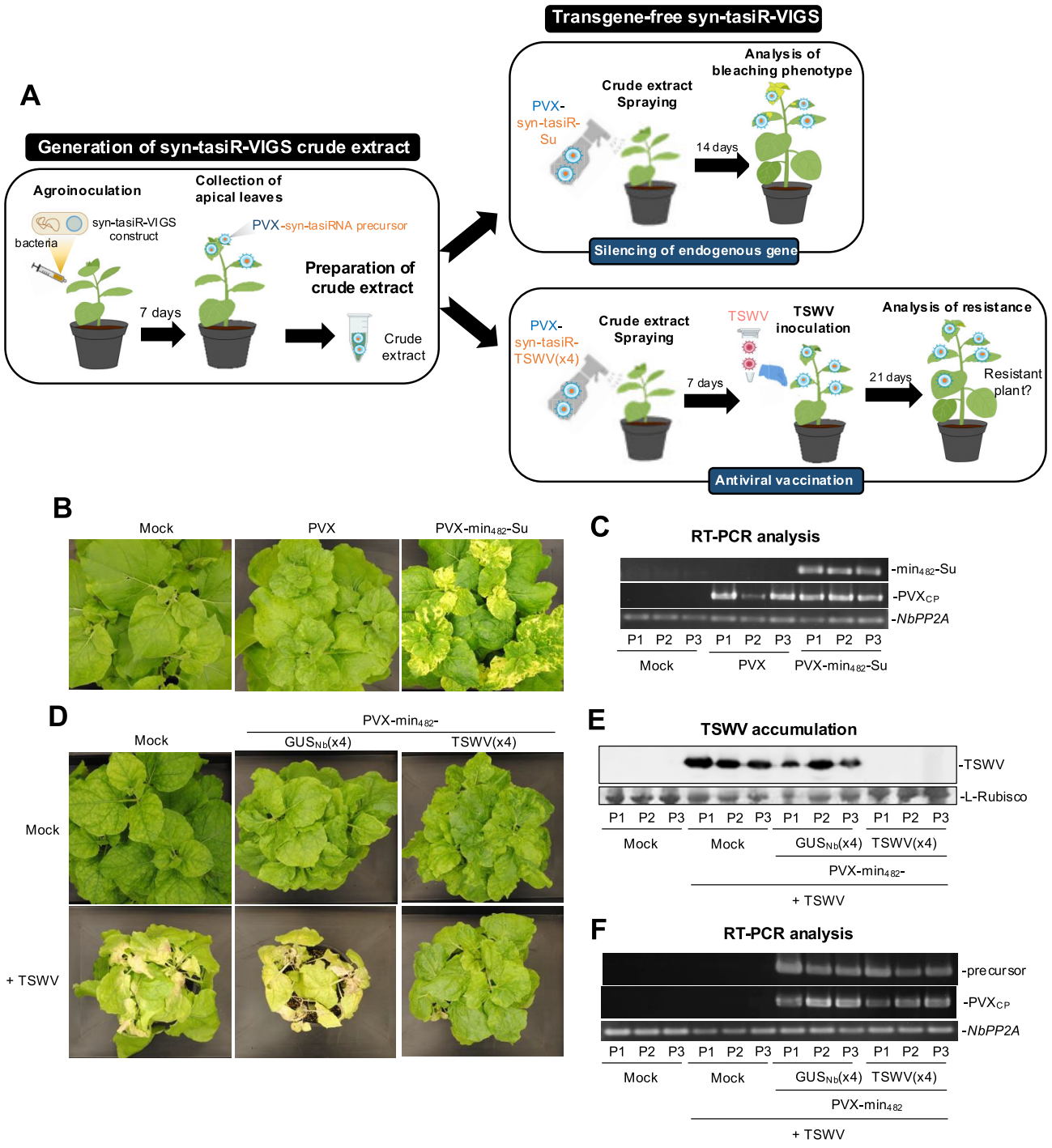

Figure 7. Transgene-free widespread gene silencing and plant antiviral vaccination through PVX-based syn-tasiR-VIGS. (**A**) Experimental procedure for transgene-free syn-tasiR-VIGS in *N. benthamiana* plants. Left: Crude extracts are prepared from plants previously agroinfiltrated with the corresponding syn-tasiR-VIGS construct. Right: Young plants are spray-inoculated with syn-tasiR-VIGS extracts to induce bleaching derived from *NbSu* silencing (top) or antiviral resistance against TSWV (bottom). (**B**) Widespread silencing of *NbSu* induced by sprayed crude extracts. Photographs at 14 days post-spray (dps) of sets of three plants sprayed with different crude extracts obtained from agroinoculated plants. (**C**) RT-PCR detection at 14 dps of min_{482}*-Su* precursors and PVX CP fragment (PVX_{CP}) in apical leaves of each of the three sprayed plants (P1–P3). RT-PCR products corresponding to the control *NbPP2A* are also shown. (**D**) Plant vaccination with syn-tasiR-VIGS extracts for immunization against TSWV. Photographs at 21 dpi of sets of three plants sprayed with different crude extracts obtained from agroinoculated plants. (**E**) Western blot detection of TSWV in protein preparations from apical leaves collected at 14 dpi of each of the three sprayed plants (P1–P3). Other details are as in Fig. 6D. (**F**) RT-PCR detection at 14 dpi of min_{482}*-TSWV(x4)* precursors and PVX CP fragment (PVX_{CP}) in apical leaves of each of the three plants sprayed (P1–P3). Other details are as in Fig. 5G.

Next, crude extracts containing *35S:PVX-min$_{482}$-TSWV(x4)* were sprayed onto three *N. benthamiana* plants, and seven days later the plants were mechanically inoculated with a TSWV infectious extract. TSWV-induce symptoms were monitored over 21 dpi. Control crude extracts from mock- and *35S:PVX-min$_{482}$-GUS$_{Nb}$(x4)*-agroinoculated plants were sprayed in parallel, and plants were inoculated with TSWV as described. Plants vaccinated with PVX-min$_{482}$-TSWV(x4) extracts did not show any TSWV symptom and did not accumulate TSWV (Fig. 7D and E), while plants treated with mock or PVX-min$_{482}$-GUS(x4) extracts displayed severe plant chlorosis and leaf epinasty and accumulated high levels of TSWV (Fig. 7D and E). As before, the presence of PVX and *min$_{482}$*-based precursors was analysed by RT-PCR (Fig. 7F), confirming that the lack of protection in plants treated with PVX-min$_{482}$-GUS$_{Nb}$(x4) extracts was not due to the absence of PVX or the loss of the syn-tasiRNA precursor. Collectively, these findings demonstrate that crude extracts can be directly sprayed onto leaves to trigger syn-tasiR-VIGS in *N. benthamiana* in a DNA-free, nontransgenic manner, enabling both silencing of endogenous genes and plant vaccination against pathogenic viruses.

Discussion

Here, we show that minimal RNA precursors consisting exclusively of a 22-nt miRNA TS and an 11-nt *AtTAS1c*-derived spacer produce high levels of accurately processed syn-tasiRNAs in different plant species for efficient gene silencing. Remarkably, minimal precursors have the unique ability to express authentic syn-tasiRNAs from an RNA viral vector such as PVX, enabling transgene-free widespread gene silencing in plants.

Effect of minimizing the precursor length on syn-tasiRNA biogenesis and function in Arabidopsis

The effect on secondary siRNA biogenesis of deleting sequences from *TAS* precursors was examined before when looking for regulatory functions of putative *cis* elements included in *TAS* sequences. For instance, the 930-nt full-length *AtTAS1a* was shortened to 252-nt by removing the 5′ region upstream of the AtmiR173a TS and/or the region downstream of the tasiRNA 3′D9[+] position [40]. None of the deleted sequences were determinant for syn-tasiRNA biogenesis, although syn-tasiRNA accumulation was negatively affected. In a different study, the 5′ region upstream of AtmiR173a TS was also deleted from *AtTAS1c* without a clear effect on syn-tasiRNA accumulation [14]. However, it was proposed that other precursor elements such as the poly(A) tail or the total transcript length may be crucial for proper syn-tasiRNA accumulation. In any case, both studies suggest that the presence of AtmiR173a TS is sufficient for triggering tasiRNA biogenesis. Indeed, phased tasiRNAs were generated from gene fragments placed downstream a AtmiR173a TS without the need for any regulatory sequences [14, 40]. Here, syn-tasiRNAs accumulated to lower levels in Arabidopsis plants expressing the minimal precursor compared to those expressing the full-length*AtTAS1c*, suggesting the existence of *cis* elements in *AtTAS1c* that positively regulate syn-tasiRNA accumulation. Remarkably, some *TAS* genes have short ORFs located immediately upstream of the tasiRNA-producing region, which are translated and trigger the synthesis of small peptides [41, 42]. Indeed, mutations affecting either the stop codon or the overall ORF length lower tasiRNA accumulation, most likely due to a decreased stability of the *TAS* precursor caused by lower protection from ribosomes [43, 44]. More recently, a model was proposed in which ribosomes start translating the ORFs and stall near the miRNA TS through the interaction with the SGS3-AGO1-miRNA complex [45]. This interaction is thought to stabilize the complex, thus increasing the amount of tasiRNA produced. In the case of the *AtTAS1c* precursor, two ORFs are located in the 5′ region upstream of the AtmiR173a TS (ORF1 and ORF2), and a third ORF overlaps with ORF2 and includes the miRNA TS [42]. These findings may explain the higher accumulation of syn-tasiR-FT and syn-tasiR-CH42 in Arabidopsis plants expressing full-length *AtTAS1c* precursors compared to those expressing ORF-deficient minimal precursors. Still, these differences in syn-tasiRNA accumulation seem to be less drastic than those reported before [14, 40], maybe because here syn-tasiRNAs are expressed from the 3′D2[+] position, which maximizes both syn-tasiRNA accumulation and gene silencing efficiency [18]. Intriguingly, syn-tasiRNAs expressed from minimal precursors accumulated to similar levels than those expressed from *AtTAS1c* in *N. benthamiana*. It is possible that *AtTAS1c* ORFs are not recognized in *N. benthamiana* (where the *TAS1c*/miR173a pathway is missing) and, consequently, full-length *AtTAS1c* precursors are not protected by ribosomes. Finally, highly phased syn-tasiRNAs were produced from minimal precursors, indicating an accurate processing of the minimal precursors that prevents off-target effects caused by misprocessed sRNA species. Indeed, phasing maintenance during the processing of the minimal precursors is consistent with previous studies indicating that phasing depends on miRNA-AGO cleavage of the *TAS* transcript rather than on any *cis* regulatory element [46].

Highly phased, accurately processed syn-tasiRNAs are produced in *N. benthamiana* with precursors including TSs from 22-nt endogenous miRNAs

The co-expression of *AtMIR173a* together with *AtTAS1c*-based syn-tasiRNA constructs is required to produce syn-tasiRNAs in non-Arabidopsis species such as *N. benthamiana* and *Solanum lycopersicum* [18, 23, 37]. Here, highly abundant and phased syn-tasiRNAs were produced in *N. benthamiana* from full-length *AtTAS1c*-based precursors including a TS from *N. benthamiana* endogenous 22-nt miRNAs. This result indicates that the AtmiR173a TS is not essential for *AtTAS1c*-dependent syn-tasiRNA biogenesis, and that alternative TSs from other 22-nt miRNAs can be used. *N. benthamiana* has seven miRNA families with 22-nt miRNA members. Among them, miR482a and miR6019a/b are present in members of the *Solanaceae* family, play roles in immune responses to pathogens, and trigger phased siRNA formation [47–50]. NbmiR482a is highly expressed in *N. benthamiana* seedlings, leaves, and stems, while NbmiR6019a/b expression in these tissues is more modest [49] (Supplementary Fig. S4). These differences in miRNA expression may explain the higher accumulation of syn-tasiRNAs produced from precursors with NbmiR482a TS. Interestingly, syn-tasiRNA accumulation from *AtTAS1c* full-length precursors and gene silencing efficiency were similar in plants overexpressing AtmiR173a and in those using NbmiR482a as the endogenous

trigger, indicating that NbmiR482a levels are not limiting. It is worth noting that miRNA expression profiles are dynamic and vary between tissues, developmental stages and during infections [51]. Therefore, selecting the appropriate miRNA as endogenous trigger may require understanding its expression pattern across tissues or under different plant growth conditions. On the other hand, the specific expression profiles of certain miRNAs may allow syn-tasiRNA biogenesis to be tissue- or condition-specific, which could be an attractive strategy to pursue in specific cases.

Transgene-free syn-tasiR-VIGS for widespread gene silencing in plants

Syn-tasiR-VIGS was developed by incorporating a minimal precursor with an endogenous 22-nt miRNA TS in the genome of a viral vector such as PVX. As previously observed with PVX-based amiR-VIGS [26], long precursors such as *AtTAS1c* (1011 nt) are not stably maintained in the viral genome for extended periods, highlighting the limited cargo capacity of viral vectors. In this context, minimal precursors offer a unique advantage due to their small size, allowing stable maintenance in the viral genome while reducing the accumulation of mutations during viral replication. Here, we used a PVX cDNA sequence with a deletion of the amino-terminal end of the CP and a heterologous promoter derived from bamboo mosaic virus [52], enhancing insert stability in PVX-based constructs. Remarkably, PVX-based syn-tasiRNAs were accurately processed from minimal precursors and accumulated to high levels, as shown by high-throughput sRNA sequencing and northern blot. Since PVX replicates in the cytoplasm, it is plausible that DCL4, a cytoplasmic DCL, is the main DCL processing syn-tasiRNA duplexes from dsRNAs generated after NbmiR482a cleavage, as occurs during the synthesis of endogenous tasiRNAs [53, 54]. On the other hand, DCL4 is considered the primary antiviral DCL [55, 56], particularly during PVX infections in *N. benthamiana* [57], and together with DCL2 and DCL3 processes viral dsRNA replicative intermediates into virus-derived siRNAs as part of the natural plant's antiviral defense. Here, sRNA sequencing confirmed the *in vivo* production of high levels of authentic 21-nt syn-tasiRNAs phased with the NbmiR482a cleavage site, with a relatively low proportion of sRNAs derived from the rest of the precursor. These results suggest that syn-tasiRNAs are produced from RDR6/SGS3-dependent dsRNAs post-NbmiR482a cleavage rather than from RDR-derived viral replicative intermediates. They also support that target silencing is a direct result of syn-tasiRNA function, not of potential siRNAs generated from the minimal precursor that might share sequence complementarity with target mRNAs. This is further supported by the lack of *NbSu* silencing observed when expressing PVX-based constructs that include AtmiR173a TS upstream the syn-tasiR-Su sequence. In any case, NbmiR482a targeting and subsequent processing of minimal precursors from PVX are efficient enough to produce high levels of syn-tasiRNAs while allowing continued PVX replication to sustain syn-tasiRNA synthesis over time and across new tissues. It is important to note that the efficacy of our syn-tasiR-VIGS approach using minimal precursors is based on the rigorous selection of validated syn-tasiRNAs with proven specificity and effectiveness [17, 20]. This compensates for the fact that only a few but highly effective syn-tasiRNAs sequences are produced, compared to other larger *TAS* systems that generate secondary siRNAs from gene fragments included after the 22-nt miRNA TS and spacer [36, 40]. In these larger systems, specitificy is compromised, as there is no control over the sequence or size of the resulting siRNAs, which may unintentionally target other cellular RNAs, potentially leading to off-target effects and unintended phenotypic consequences.

A key feature of syn-tasiR-VIGS is its scalability and non-transgenic application via the spraying of plant leaves with infectious crude extracts from plants accumulating the viral vector with the minimal precursor, as shown recently for PVX-based amiR-VIGS [26]. Previously, syn-tasiRNAs were expressed from transgenic tissues, which limited their practical applications due to commercial and/or regulatory constraints. Another common limitation of the syn-tasiRNA technology has been the need of co-expressing AtmiR173a together with *AtTAS1c*-based constructs in non-Arabidopsis species. The finding that authentic syn-tasiRNAs can be efficiently produced from minimal precursors consisting exclusively of an endogenous 22-nt miRNA TS and an 11-nt spacer significantly broadens the biotechnological applications of syn-tasiRNAs. Moreover, the new set of 'B/c' plasmids listed in Supplementary Fig. S8 simplifies in a time- and cost-effective manner the generation of constructs containing minimal syn-tasiRNA precursors, especially when combined with high-throughput cloning methodologies that eliminate the need for gel purification and amplification steps, employing zero-background and Golden Gate strategies [16].

Future research efforts should focus on further developing syn-tasiR-VIGS across different areas. First, it is important to test other viral vectors with broader or species-specific host ranges to adapt syn-tasiR-VIGS to different plant species, including crops. Second, efforts should aim to minimize viral vector pathogenicity by introducing mutations or deletions to attenuate viral symptoms while preserving systemic movement and replication. Third, alternative delivery methods beyond spray application could be developed for specific crops, such as mechanical or insect-mediated inoculation and root absorption. Still, the general use of VIGS in crops presents several controversial aspects [58]: (i) the efficiency of VIGS can vary significantly between plant species, tissues and environmental conditions, leading to inconsistent results and limiting large-scale application; (ii) VIGS-induced silencing can result in unintended phenotypic changes due to off-target effects, transcriptomic alterations or viral vector interactions with the host plant's defense mechanisms; (iii) prolonged activation of the RNA silencing machinery in response to viral infection can lead to growth retardation and yield reduction, making it less practical for commercial crops; (iv) VIGS vectors may mutate or lose inserted sequences during prolonged infections, compromising their efficacy; and (v) the potential environmental release of genetically modified viral vectors used in VIGS raises biosafety concerns regarding their unintended spread to nontarget species and ecosystems, prompting regulatory restrictions on their agricultural application due to genetic modification and ecological impact concerns. In this context, transgene-free alternatives for syn-tasiRNA expression in plants, such as the topical delivery of syn-tasiRNA precursor molecules or the expression of syn-tasiRNAs from CRISPR/Cas-edited endogenous secondary siRNA-generating loci, should be explored to overcome these limitations.

New generation of antiviral vaccines based on syn-tasiR-VIGS

Traditional antiviral vaccines for plants rely on cross-protection, where a mild or attenuated virus strain protects the plant against more severe strains of the same or a closely related virus [59]. However, identifying mild strains for a particular virus may can be challenging, and their protective effect is not always guaranteed. Moreover, cross-protection is limited to closed related viruses and does not defend against distantly related or unrelated viruses, limiting its effectiveness in fields with diverse viral populations. Here, we developed of a new generation of antiviral vaccines for plants based on syn-tasiR-VIGS, which can be applied in a non-transgenic and single-dose manner. Using PVX as viral vector, we vaccinated *N. benthamiana* plants for complete immunization against an entirely unrelated virus, TSWV, one of the top 10 plant viruses based on scientific/economic importance [39]. Vaccination consisted in inoculating plants with PVX crude extracts, allowing the virus to spread and produce anti-TSWV syn-tasiRNAs throughout the plant. When a few days later TSWV is inoculated, vaccinated plants were loaded with antiviral syn-tasiRNAs that targeted TSWV and ultimately blocked its infection. Syn-tasiR-VIGS vaccines offer several advantages over traditional vaccines: (i) syn-tasiRNAs can be designed *a la carte* against any virus of interest; (ii) they may be applicable to any host-virus combination, as long as the viral vector can infect the host; and (iii) they could protect against multiple unrelated viruses by multiplexing different antiviral syn-tasiRNAs in the same minimal precursor. However, both the viral vector and the target RNA viruses may mutate during prolonged infection stages, potentially compromising syn-tasiRNA biogenesis or efficacy and enabling the target virus to evade the antiviral effects of syn-tasiRNAs, thereby limiting the long-term effectiveness of syn-tasiR-VIGS vaccines. Further research in these areas should expand the applications of syn-tasiR-VIGS vaccines and position them as a next-generation antiviral strategy for protecting plants against pathogenic viruses.

Acknowledgements

We thank José-Antonio Daròs (IBMCP) for sharing the *pLBPVXBa-M* plasmid, Javier Forment (IBMCP) for his assistance with the sRNA sequencing data analysis, and the greenhouse staff at IBMCP for their help in maintaining the plants.

Author contributions: A.E.C. and A.A.G. did most of the experimental work with the help of J.L.G., M.J.M., A.P.E., and A.P. A.E.C., A.A.G., and A.C. analysed the data. A.C. conceived the research, supervised the project, and wrote the manuscript with input from the rest of authors.

Supplementary data

Supplementary data is available at NAR online.

Conflict of interest

None declared.

Funding

This work was supported by grants or fellowships from MCIN/AEI/10.13039/501 100 011 033 and/or by the 'European Union NextGenerationEU/PRTR' [PID2021-122186OB-100, CNS2022-135107 and RYC-2017-21648 to A.C.; PRE2019-088439, PRE2022-102565, and PRE2022-103177 to A.E.C., J.L.G., and M.J.M, respectively], from Consejo Superior de Investigaciones Científicas (CSIC, Spain) [JAEINT_20_01312 to A.P.E.], and from European Commission [Erasmus + Grant Agreement 2020-1-DE01-KA103-005653 to A.P.].

Data availability

All original data will be made available upon request. High-throughput sequencing data can be found in the Sequence Read Archive (SRA) database under accession number PRJNA1172601. New B/c and PVX vectors are available from Addgene: *pENTR-B/c* (Addgene plasmid #227 962, https://www.addgene.org/227962), *pMDC32B-B/c* (Addgene plasmid #227 963, https://www.addgene.org/227963), *pENTR-AtmiR173aTS-B/c* (Addgene plasmid #227 964, https://www.addgene.org/227964), *pMDC32B-AtmiR173aTS-B/c* (Addgene plasmid #227 965, https://www.addgene.org/227965), *pENTR-NbmiR482aTS-B/c* (Addgene plasmid #227 966, https://www.addgene.org/227966), *pMDC32B-NbmiR482aTS-B/c* (Addgene plasmid #227 967, https://www.addgene.org/227967).

References

1. Fire A, Xu S, Montgomery MK *et al.* Potent and specific genetic interference by double-stranded RNA in *Caenorhabditis elegans*. *Nature* 1998;**391**:806–11. https://doi.org/10.1038/35888
2. Bernstein E, Caudy AA, Hammond SM *et al.* Role for a bidentate ribonuclease in the initiation step of RNA interference. *Nature* 2001;**409**:363–6. https://doi.org/10.1038/35053110
3. Hammond SM, Bernstein E, Beach D *et al.* An RNA-directed nuclease mediates post-transcriptional gene silencing in Drosophila cells. *Nature* 2000;**404**:293–6. https://doi.org/10.1038/35005107
4. Jackson AL, Bartz SR, Schelter J *et al.* Expression profiling reveals off-target gene regulation by RNAi. *Nat Biotechnol* 2003;**21**:635–7. https://doi.org/10.1038/nbt831
5. Carbonell A. Artificial small RNA-based strategies for effective and specific gene silencing in plants. In: Dalmay T (ed.), *Plant Gene Silencing: Mechanisms and Applications*. Wallingford, UK: CABI Publishing, 2017, 110–27.
6. Carbonell A. Secondary small interfering RNA-based silencing tools in plants: an update. *Front Plant Sci* 2019;**10**:687. https://doi.org/10.3389/fpls.2019.00687
7. Zhang ZJ. Artificial trans-acting small interfering RNA: a tool for plant biology study and crop improvements. *Planta* 2014;**239**:1139–46. https://doi.org/10.1007/s00425-014-2054-x
8. Cuperus JT, Carbonell A, Fahlgren N *et al.* Unique functionality of 22-nt miRNAs in triggering RDR6-dependent siRNA biogenesis from target transcripts in Arabidopsis. *Nat Struct Mol Biol* 2010;**17**:997–1003. https://doi.org/10.1038/nsmb.1866
9. Chen H-M, Chen L-T, Patel K *et al.* 22-nucleotide RNAs trigger secondary siRNA biogenesis in plants. *Proc Natl Acad Sci USA* 2010;**107**:15269–74. https://doi.org/10.1073/pnas.1001738107
10. Allen E, Xie Z, Gustafson AM *et al.* microRNA-directed phasing during trans-acting siRNA biogenesis in plants. *Cell* 2005;**121**:207–21. https://doi.org/10.1016/j.cell.2005.04.004
11. Yoshikawa M, Peragine A, Park MY *et al.* A pathway for the biogenesis of trans-acting siRNAs in Arabidopsis. *Genes Dev* 2005;**19**:2164–75. https://doi.org/10.1101/gad.1352605
12. Li J, Yang Z, Yu B *et al.* Methylation protects miRNAs and siRNAs from a 3'-end uridylation activity in Arabidopsis. *Curr Biol* 2005;**15**:1501–7. https://doi.org/10.1016/j.cub.2005.07.029

13. Montgomery TA, Howell MD, Cuperus JT *et al.* Specificity of ARGONAUTE7-miR390 interaction and dual functionality in TAS3 trans-acting siRNA formation. *Cell* 2008;**133**:128–41. https://doi.org/10.1016/j.cell.2008.02.033
14. Montgomery TA, Yoo SJ, Fahlgren N *et al.* AGO1-miR173 complex initiates phased siRNA formation in plants. *Proc Natl Acad Sci USA* 2008;**105**:20055–62. https://doi.org/10.1073/pnas.0810241105
15. Lunardon A, Kariuki SM, Axtell MJ. Expression and processing of polycistronic artificial microRNAs and trans-acting siRNAs from transiently introduced transgenes in *Solanum lycopersicum* and *Nicotiana benthamiana*. *Plant J* 2021;**106**:1087–104. https://doi.org/10.1111/tpj.15221
16. Carbonell A, Takeda A, Fahlgren N *et al.* New generation of artificial microRNA and synthetic trans-acting small interfering RNA vectors for efficient gene silencing in Arabidopsis. *Plant Physiol* 2014;**165**:15–29. https://doi.org/10.1104/pp.113.234989
17. Cisneros AE, de la Torre-Montaña A, Carbonell A. Systemic silencing of an endogenous plant gene by two classes of mobile 21-nucleotide artificial small RNAs. *Plant J* 2022;**110**:1166–81. https://doi.org/10.1111/tpj.15730
18. López-Dolz L, Spada M, Daròs J-A *et al.* Fine-tune control of targeted RNAi efficacy by plant artificial small RNAs. *Nucleic Acids Res* 2020;**48**:6234–50. https://doi.org/10.1093/nar/gkaa343
19. Carbonell A, Daròs J-A. Artificial microRNAs and synthetic trans-acting small interfering RNAs interfere with viroid infection. *Mol Plant Pathol* 2017;**18**:746–53. https://doi.org/10.1111/mpp.12529
20. Carbonell A, Lopez C, Daròs J-A. Fast-forward identification of highly effective artificial small RNAs against different tomato spotted wilt virus isolates. *Mol Plant Microbe Interact* 2019;**32**:142–56. https://doi.org/10.1094/MPMI-05-18-0117-TA
21. Cisneros AE, de la Torre-Montaña A, Martín-García T *et al.* Artificial small RNAs for functional genomics in plants. In: Tang G., Teotia S., Tang X., Singh D (eds.), *RNA-Based Technologies for Functional Genomics in Plants, Concepts and Strategies in Plant Sciences*. Cham: Springer International Publishing, 2021, 1–29.
22. Fahlgren N, Hill ST, Carrington JC *et al.* P-SAMS: a web site for plant artificial microRNA and synthetic trans-acting small interfering RNA design. *Bioinformatics* 2016;**32**:157–8. https://doi.org/10.1093/bioinformatics/btv534
23. Baykal U, Liu H, Chen X *et al.* Novel constructs for efficient cloning of sRNA-encoding DNA and uniform silencing of plant genes employing artificial trans-acting small interfering RNA. *Plant Cell Rep* 2016;**35**:2137–50. https://doi.org/10.1007/s00299-016-2024-9
24. López-Dolz L, Spada M, Daròs J-A *et al.* Fine-tuning plant gene expression with synthetic trans-acting small interfering RNAs. *Methods Mol Biol* 2022;**2408**:227–42. https://doi.org/10.1007/978-1-0716-1875-2_15
25. Su W, Xu M, Radani Y *et al.* Technological development and application of plant genetic transformation. *Int J Mol Sci* 2023;**24**:10646. https://doi.org/10.3390/ijms241310646
26. Cisneros AE, Martín-García T, Primc A *et al.* Transgene-free, virus-based gene silencing in plants by artificial microRNAs derived from minimal precursors. *Nucleic Acids Res* 2023;**51**:10719–36. https://doi.org/10.1093/nar/gkad747
27. Clough SJ, Bent AF. Floral dip: a simplified method for Agrobacterium-mediated transformation of *Arabidopsisthaliana*. *Plant J* 1998;**16**:735–43. https://doi.org/10.1046/j.1365-313x.1998.00343.x
28. Schwab R, Ossowski S, Riester M *et al.* Highly specific gene silencing by artificial microRNAs in Arabidopsis. *Plant Cell* 2006;**18**:1121–33. https://doi.org/10.1105/tpc.105.039834
29. Curtis MD, Grossniklaus U. A gateway cloning vector set for high-throughput functional analysis of genes in planta. *Plant Physiol* 2003;**133**:462–9. https://doi.org/10.1104/pp.103.027979
30. Uranga M, Aragonés V, García A *et al.* RNA virus-mediated gene editing for tomato trait breeding. *Hortic Res* 2024;**11**:uhad279. https://doi.org/10.1093/hr/uhad279
31. Aragonés V, Aliaga F, Pasin F *et al.* Simplifying plant gene silencing and genome editing logistics by a one-Agrobacterium system for simultaneous delivery of multipartite virus vectors. *Biotechnol J* 2022;**17**:2100504. https://doi.org/10.1002/biot.202100504
32. Llave C, Xie Z, Kasschau KD *et al.* Cleavage of scarecrow-like mRNA targets directed by a class of Arabidopsis miRNA. *Science* 2002;**297**:2053–6. https://doi.org/10.1126/science.1076311
33. Carbonell A, Fahlgren N, Mitchell S *et al.* Highly specific gene silencing in a monocot species by artificial microRNAs derived from chimeric miRNA precursors. *Plant J* 2015;**82**:1061–75. https://doi.org/10.1111/tpj.12835
34. Felippes FF, Wang JW, Weigel D. MIGS: miRNA-induced gene silencing. *Plant J* 2012;**70**:541–7.
35. de la L, Gutierrez-Nava M, Aukerman MJ *et al.* Artificial trans-acting siRNAs confer consistent and effective gene silencing. *Plant Physiol* 2008;**147**:543–51.
36. Zhao X, Gao Q, Wang H *et al.* syn-tasiRnas targeting the coat protein of potato virus Y confer antiviral resistance in *Nicotiana benthamiana*. *Plant Signal Behav* 2024;**19**:2358270.
37. Carbonell A, Lisón P, Daròs J-A. Multi-targeting of viral RNAs with synthetic trans-acting small interfering RNAs enhances plant antiviral resistance. *Plant J* 2019;**100**:720–37. https://doi.org/10.1111/tpj.14466
38. Ratcliff F, Martin-Hernandez AM, Baulcombe DC. Technical advance: Tobacco rattle virus as a vector for analysis of gene function by silencing. *Plant J* 2001;**25**:237–45. https://doi.org/10.1046/j.0960-7412.2000.00942.x
39. Scholthof KB, Adkins S, Czosnek H *et al.* Top 10 plant viruses in molecular plant pathology. *Mol Plant Pathol* 2011;**12**:938–54. https://doi.org/10.1111/j.1364-3703.2011.00752.x
40. Felippes FF, Weigel D. Triggering the formation of tasiRNAs in *Arabidopsis thaliana*: the role of microRNA miR173. *EMBO Rep* 2009;**10**:264–70. https://doi.org/10.1038/embor.2008.247
41. de Felippes FF. Gene regulation mediated by microRNA-triggered secondary small RNAs in plants. *Plants (Basel)* 2019;**8**:112.
42. Wu H-YL, Ai Q, Teixeira RT *et al.* Improved super-resolution ribosome profiling reveals prevalent translation of upstream ORFs and small ORFs in Arabidopsis. *Plant Cell* 2024;**36**:510–39. https://doi.org/10.1093/plcell/koad290
43. Yoshikawa M, Iki T, Numa H *et al.* A short open reading frame encompassing the microRNA173 target site plays a role in trans-acting small interfering RNA biogenesis. *Plant Physiol* 2016;**171**:359–68. https://doi.org/10.1104/pp.16.00148
44. Bazin J, Baerenfaller K, Gosai SJ *et al.* Global analysis of ribosome-associated noncoding RNAs unveils new modes of translational regulation. *Proc Natl Acad Sci USA* 2017;**114**:E10018–27. https://doi.org/10.1073/pnas.1708433114
45. Iwakawa H, Lam AYW, Mine A *et al.* Ribosome stalling caused by the Argonaute-microRNA-SGS3 complex regulates the production of secondary siRNAs in plants. *Cell Rep* 2021;**35**:109300. https://doi.org/10.1016/j.celrep.2021.109300
46. Arribas-Hernandez L, Marchais A, Poulsen C *et al.* The slicer activity of ARGONAUTE1 Is required specifically for the phasing, not production, of trans-acting short interfering RNAs in Arabidopsis. *Plant Cell* 2016;**28**:1563–80.
47. Li F, Pignatta D, Bendix C *et al.* MicroRNA regulation of plant innate immune receptors. *Proc Natl Acad Sci USA* 2012;**109**:1790–5. https://doi.org/10.1073/pnas.1118282109
48. Shivaprasad PV, Chen H-M, Patel K *et al.* A microRNA superfamily regulates nucleotide binding site-leucine-rich repeats and other mRNAs. *Plant Cell* 2012;**24**:859–74. https://doi.org/10.1105/tpc.111.095380
49. Baksa I, Nagy T, Barta E *et al.* Identification of *Nicotiana benthamiana* microRNAs and their targets using high throughput sequencing and degradome analysis. *BMC Genomics* 2015;**16**:1025. https://doi.org/10.1186/s12864-015-2209-6

50. Deng P, Muhammad S, Cao M *et al.* Biogenesis and regulatory hierarchy of phased small interfering RNAs in plants. *Plant Biotechnol J* 2018;**16**:965–75. https://doi.org/10.1111/pbi.12882
51. Jones-Rhoades MW, Bartel DP, Bartel B. MicroRNAS and their regulatory roles in plants. *Annu Rev Plant Biol* 2006;**57**:19–53. https://doi.org/10.1146/annurev.arplant.57.032905.105218
52. Dickmeis C, Fischer R, Commandeur U. Potato virus X-based expression vectors are stabilized for long-term production of proteins and larger inserts. *Biotechnol J* 2014;**9**:1369–79. https://doi.org/10.1002/biot.201400347
53. Gasciolli V, Mallory AC, Bartel DP *et al.* Partially redundant functions of Arabidopsis DICER-like enzymes and a role for DCL4 in producing trans-acting siRNAs. *Curr Biol* 2005;**15**:1494–500. https://doi.org/10.1016/j.cub.2005.07.024
54. Xie Z, Allen E, Wilken A *et al.* DICER-LIKE 4 functions in trans-acting small interfering RNA biogenesis and vegetative phase change in *Arabidopsis thaliana*. *Proc Natl Acad Sci USA* 2005;**102**:12984–9. https://doi.org/10.1073/pnas.0506426102
55. Deleris A, Gallego-Bartolome J, Bao J *et al.* Hierarchical action and inhibition of plant Dicer-like proteins in antiviral defense. *Science* 2006;**313**:68–71. https://doi.org/10.1126/science.1128214
56. Bouche N, Lauressergues D, Gasciolli V *et al.* An antagonistic function for Arabidopsis DCL2 in development and a new function for DCL4 in generating viral siRNAs. *EMBO J* 2006;**25**:3347–56. https://doi.org/10.1038/sj.emboj.7601217
57. Andika IB, Maruyama K, Sun L *et al.* Differential contributions of plant Dicer-like proteins to antiviral defences against potato virus X in leaves and roots. *Plant J* 2015;**81**:781–93.
58. Rössner C, Lotz D, Becker A. VIGS goes viral: how VIGS transforms our understanding of plant science. *Annu Rev Plant Biol* 2022;**73**:703–28. https://doi.org/10.1146/annurev-arplant-102820-020542
59. Ziebell H, Carr JP. Chapter 6 - cross-protection: a century of mystery. In: Carr JP, Loebenstein G (eds.), *Advances in Virus Research, Natural and Engineered Resistance to Plant Viruses, Part II*. Vol. **76**. Cambridge, Massachusetts, USA: Academic Press, 2010, 211–64.

Received: December 2, 2024. **Revised:** January 22, 2025. **Editorial Decision:** February 18, 2025. **Accepted:** February 24, 2025